JOURNAL OF PETROLOGY | VOLUME 38 | NUMBER 9 | PAGES 1113–1135 | 1997

Liquid Immiscibility in the Join $NaAlSiO_4$–$NaAlSi_3O_8$–$CaCO_3$ at 1 GPa: Implications for Crustal Carbonatites

WOH-JER LEE* AND PETER J. WYLLIE

DIVISION OF GEOLOGICAL AND PLANETARY SCIENCES, CALIFORNIA INSTITUTE OF TECHNOLOGY, PASADENA, CA 91125, USA

RECEIVED NOVEMBER 8, 1996; REVISED TYPESCRIPT ACCEPTED APRIL 11, 1997

The synthetic system Na_2O–CaO–Al_2O_3–SiO_2–CO_2 has been widely used as a model to show possible relationships among alkalic silicate magmas, calciocarbonatites, and natrocarbonatites. The determined immiscibility between silicate- and carbonate-rich liquids has been strongly advocated to explain the formation of natural carbonatite magmas. Phase fields intersected at 1·0 GPa by the composition joins $NaAlSiO_3O_8$–$CaCO_3$ (Ab–CC, published) and $NaAlSiO_4(Ne)_{90}Ab_{10}$–CC (new), along with measured immiscible liquid compositions, provide pseudoternary phase relationships for the composition triangles Ab–CC–Na_2CO_3(NC) and $Ne_{90}Ab_{10}$–CC–NC. Interpolation between these, and extrapolation within the CO_2-saturated tetrahedron Al_2O_3–SiO_2–CaO–Na_2O, provides pseudoquaternary phase relationships defining the volume for the miscibility gap and the surface for the silicate–carbonate liquidus field boundary. The miscibility gap extends between 10 and 70 wt % $CaCO_3$ on the triangle Ne–Ab–CC at 1·0 GPa; it does not extend to the Na_2O-free side of the tetrahedron. The liquidus minerals in equilibrium with both silicate- and carbonate-rich consolute liquids are nepheline, plagioclase, melilite, and wollastonite; with increasing Si/Al the liquidus for calcite reaches the miscibility gap. We use these phase relationships to: (1) illustrate possible paths of crystallization of initial CO_2-bearing silicate haplomagmas, (2) place limits on the compositions of immiscible carbonatite magmas which can be derived from silicate parent magmas, and (3) illustrate paths of crystallization of carbonatite magmas. Cooling silicate–CO_2 liquids may reach the miscibility gap, or the silicate–calcite liquidus field boundary, or terminate at a eutectic precipitating silicates and giving off CO_2. Silicate–CO_2 liquids can exsolve liquids ranging from $CaCO_3$-rich to alkalic carbonate compositions. There is no basis in phase relationships for the occurrence of calciocarbonatite magmas with ~99 wt % $CaCO_3$; carbonate liquids derived by immiscibility from a silicate–CO_2 parent (at crustal pressures) contain a maximum of 80 wt % $CaCO_3$. There are two relevant paths for a silicate liquid which exsolves carbonate-rich liquid (along with silicate mineral precipitates): (1) the assemblage is joined by calcite, or (2) the assemblage persists without carbonate precipitation until all silicate liquid is used up. The phase diagrams indicate that high-temperature immiscible carbonate-rich liquids must be physically separated from parent silicate liquid before they can precipitate carbonate-rich mineral assemblages. Path (1) then corresponds to the silicate–calcite liquidus field boundary, and a stage is reached where the carbonate-rich liquids will precipitate large amounts of calcite and fractionate toward alkali carbonates (not necessarily matching natrocarbonatite compositions). In path (2) the high-temperature immiscible carbonate liquid precipitates only silicates through a temperature interval until it reaches the silicate–carbonate liquidus field boundary, where it may precipitate calcite or nyerereite or gregoryite. Sövites are readily explained as cumulates, with residual alkali-rich melts causing fenitization. We can see no way in phase diagrams for vapor loss to remove alkalis and change immiscible natrocarbonatite liquids to $CaCO_3$-rich liquids; adjustments to vapor loss would be made not by change in liquid composition but by precipitation of calcite and silicate minerals. The processes illustrated in this model system are applicable to a wide range of magmatic conditions, and they complement and facilitate interpretation of phase relationships in the single paths represented by each whole-rock phase equilibrium study.

KEY WORDS: *calciocarbonatite; join $NaAlSiO_4$–$NaAlSi_3O_8$–$CaCO_3$; liquid immiscibility; natrocarbonatite*

*Corresponding author. Telephone: (626)-395-6239. Fax: (626)-568-0935. e-mail: wjl@gps.caltech.edu

INTRODUCTION

The simplest synthetic system representing extrusive natrocarbonatites, intrusive calcic carbonatites, and associated alkalic igneous rocks is the five-component system Na_2O–CaO–Al_2O_3–SiO_2–CO_2. However, this system requires three dimensions for complete graphical representation with excess CO_2 (Fig. 1). The utility of phase relationships in such model systems as a guide to possible processes in natural systems, and for interpretation of phase equilibrium studies of more complex rock systems, was recently discussed and justified by Lee & Wyllie (1996). The topology of liquidus surfaces and field boundaries elucidates possible processes, although the precise details vary, as the relative positions of field boundaries vary with pressure (Lee & Wyllie, 1996, 1997), and with composition [e.g. with peralkalinity (Kjarsgaard & Peterson, 1991) and with added MgO (Lee & Wyllie, 1997)].

The natrocarbonatite lava flows of Oldoinyo Lengai, the only observed carbonatite magmas, constitute a small fraction of a large pile of nephelinite and phonolite tephra, with subordinate lavas (Dawson *et al.*, 1994, 1996; Church & Jones, 1995; Barker, 1996*a*). Barker (1996*a*) described examples from the estimated 50 volcanic carbonatites known worldwide from catalogues (Woolley, 1987; Kogarko *et al.*, 1995*b*) of carbonatite occurrences. Calcite-rich lapilli in tephra provide evidence for calcic carbonatite magmas (Keller, 1981, 1989); associated volcanic rocks are commonly nephelinites and phonolites (Barker, 1996*a*) or melilitites (Stoppa & Lavecchia, 1992). It is widely held that intrusive calciocarbonatites are relatively minor components emplaced late into igneous complexes dominated by alkalic rocks (Heinrich, 1966; Tuttle & Gittins, 1966; Le Bas, 1977; Barker, 1989; Bell, 1989). Bailey (1993) presented a stimulating review giving examples of calciocarbonatites which were not dominated by alkalic rocks, suggesting that some of them represented primary magmas from the mantle.

It is well established experimentally that the composition of magma from carbonated peridotite does not correspond to calciocarbonatite, but to a calcic dolomitic magma with silica and alkali content depending on the host peridotite composition (Wyllie & Huang, 1975, 1976; Eggler, 1976, 1978; Wyllie, 1978; Wallace & Green, 1988; Thibault *et al.*, 1992; Dalton & Wood, 1993; Sweeney, 1994). Dalton & Wood (1993) presented experimental results indicating that repeated metasomatism of wehrlite by primary dolomitic carbonatite melt could yield a more calcic magma, and this evidence has been applied in petrogenetic arguments by Bailey (1993), Kogarko *et al.* (1995*a*), and Barker (1996*b*). However, Lee & Wyllie (1997) pointed out that the enrichment in calcite must be limited by the position of the silicate–carbonate field boundary (Wyllie & Huang, 1976, fig. 11; Eggler, 1978, fig. 13), and by the composition of a near-invariant liquid with coexisting olivine, clinopyroxene and calcic carbonate [6y in fig. 11d of Wyllie & Huang (1976)].

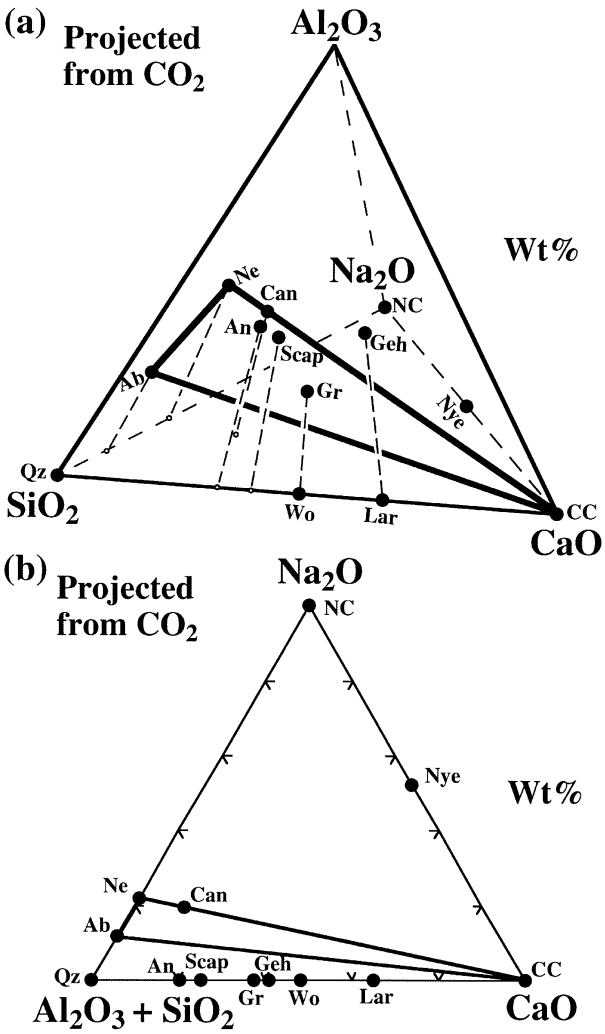

Fig. 1. Compositional tetrahedron Al_2O_3–SiO_2–CaO–Na_2O, projected from CO_2, showing silicate and carbonate phases relevant to the system Na_2O–CaO–Al_2O_3–SiO_2–CO_2. ●, compositions of these phases. Ab, albite; Ne, nepheline; An, anorthite; Gr, grossular; Wo, wollastonite; Scap, scapolite; Lar, larnite; Geh, gehlenite; Can, cancranite; CC, calcite; Nye, nyerereite; NC, sodium carbonate. ○, projection of the phases on the basal triangle SiO_2–CaO–Na_2O from Al_2O_3. The bold triangle indicates the studied join Ne–Ab–CC. (b) Compositional triangle ($Al_2O_3 + SiO_2$)–CaO–Na_2O ($+CO_2$; Hamilton projection), showing the same silicate and carbonate phases (●). Our starting mixtures lie slightly below line Ne–CC, with 10 wt % Ab in the bulk silicate material.

Phase equilibrium studies of silicate–carbonate liquidus relationships include experiments using natural rocks (Koster van Groos, 1975; Freestone & Hamilton, 1980; Baker & Wyllie, 1990; Kjarsgaard & Peterson, 1991; Hamilton & Kjarsgaard, 1993; Kjarsgaard *et al.*, 1995; Lee & Wyllie, 1997), and synthetic systems (Wyllie &

Haas, 1965; Koster van Groos & Wyllie, 1966, 1968, 1973; Franz & Wyllie, 1967; Boettcher & Wyllie, 1969; Watkinson & Wyllie, 1969, 1971; Eggler, 1974, 1976, 1978; Huang & Wyllie, 1974; Maaloe & Wyllie, 1975; Wyllie & Huang, 1975, 1976; Verwoerd, 1978; Huang *et al.*, 1980; Kjarsgaard & Hamilton, 1988, 1989; Brooker & Hamilton, 1990; Hamilton & Kjarsgaard, 1993; Otto & Wyllie, 1993; Lee & Wyllie, 1994, 1996; Lee *et al.*, 1994). In particular, experimental results on composition joins through the system Na_2O–CaO–Al_2O_3–SiO_2–CO_2 (with and without H_2O) have been published by Koster van Groos & Wyllie (1966, 1968, 1973), Watkinson & Wyllie (1969, 1971), Watkinson (1970), Kjarsgaard & Hamilton (1988, 1989), Brooker & Hamilton (1990), Hamilton & Kjarsgaard (1993), and Lee & Wyllie (1994, 1996). Most of these investigations reported a miscibility gap between silicate and carbonate liquids.

Lee & Wyllie (1992*a*, *b*, 1996) presented a detailed study of the join $NaAlSi_3O_8$–$CaCO_3$ between 1·0 and 2·5 GPa. To expand the coverage and to define more closely the phase relationships on the silicate and carbonate liquidus surfaces, we present here the results for the join between 90 wt % $NaAlSiO_4$–10 wt % $NaAlSi_3O_8$ and $CaCO_3$ at 1·0 GPa. The paths of crystallization in model systems, and the resultant parageneses and liquid compositions so derived, do not correspond precisely in terms of temperature and phase compositions to minerals and liquids in complex whole-rock systems. However, rock systems are complex, and it is not always easy to decipher the phase relationships throughout the temperature interval of interest, especially in systems where liquids do not quench to homogeneous glasses. Phase relationships for a specific rock composition represent one path through a multicomponent system, and considering the diversity of igneous rock compositions, there are many different paths to be determined. A multicomponent model phase diagram, although not representing precisely individual rock compositions, provides the broad framework of phase fields through which individual magma paths must pass, and complements and facilitates interpretation of the whole-rock experimental studies.

THE SYSTEM Na_2O–CaO–Al_2O_3–SiO_2–CO_2

The phase relationships can be presented in the tetrahedron Al_2O_3–SiO_2–CaO–Na_2O with excess CO_2 (Fig. 1a), and in the Hamilton projection (Fig. 1b) used by Freestone & Hamilton (1980): ($Al_2O_3 + SiO_2$)–CaO–Na_2O. Figure 1 shows the compositions of relevant silicate and carbonate minerals, and the bold triangle shows the composition joins Ab–CC and Ne–CC. The reader should note the different ratios of Al_2O_3/SiO_2 in Ab and Ne in Fig. 1a, which are not depicted in the Hamilton projection (Fig. 1b). Our experimental results correspond to the phase fields intersected by two triangular slices through the tetrahedron in Fig. 1a, slices which include the planes Ab–CC–NC and $Ne_{90}Ab_{10}$–CC–NC (very close to Ne–CC–NC). It turns out that the immiscible liquid compositions encountered lie very close to these projected joins.

Figure 2 shows the results of Lee & Wyllie (1996) for the Ab–CC–NC slice at 1·0 GPa based on new data for Ab–CC, and other data available for bounding systems. Noteworthy features are: (1) the immiscible two-liquid field, or miscibility gap, surrounded by the field boundaries m–I_5–k–I_5'–n; (2) the two liquidus surfaces for the precipitation of carbonates or of silicates, the latter divided by the miscibility gap into two portions, m–I_5–p–e–($Al_2O_3 + SiO_2$) and n–I_5'–o (each liquidus surface is subdivided by many field boundaries, which are not depicted); (3) the position of the silicate–carbonate liquidus field boundary e–p–I_5–I_5'–o, which is also divided into two parts by the miscibility gap; (4) the special tieline I_5–I_5'. It should be noted that although the immiscible liquids along I_5'–n are very carbonate rich, they precipitate primary silicates, and only at lower temperatures along the silicate–carbonate field boundary I_5'–o are carbonate minerals coprecipitated. The closure of the miscibility gap at critical point k should also be noted.

Earlier experimental studies reported the miscibility gap closing before reaching the Na_2O-free side of the system, but Kjarsgaard & Hamilton (1988, 1989) and Brooker & Hamilton (1990) reported a wider miscibility gap extending to the Na_2O-free side of the system, with immiscible liquids containing ~99 wt % $CaCO_3$. This has been cited by many petrologists as evidence supporting the existence of almost pure $CaCO_3$ magmas, a conclusion which is no longer tenable. Lee *et al.* (1994) and Lee & Wyllie (1996) presented evidence that the rounded calcite globules interpreted as immiscible liquids were in fact crystalline during their experiments, and defined the miscibility gap showing carbonate-rich liquids with a maximum of 80 wt % $CaCO_3$ (Fig. 2). Kjarsgaard & Hamilton (in Macdonald *et al.*, 1993, fig. 5) reinterpreted their experiments and presented a similar miscibility gap.

Lee & Wyllie (1994) showed that with H_2O added to the join $Ne_{90}Ab_{10}$–CC, the liquidus temperature was lowered sufficiently for the silicate–carbonate field boundary to pass underneath the high-temperature miscibility gap. This confirmed and explained the result of Watkinson & Wyllie (1971) for the join Ne–CC–H_2O, given the result of Kjarsgaard & Hamilton (1988) that a miscibility gap in the dry system straddled their composition join.

Koster van Groos & Wyllie (1966, 1968, 1973) explored the phase relationships on the liquidus surface around

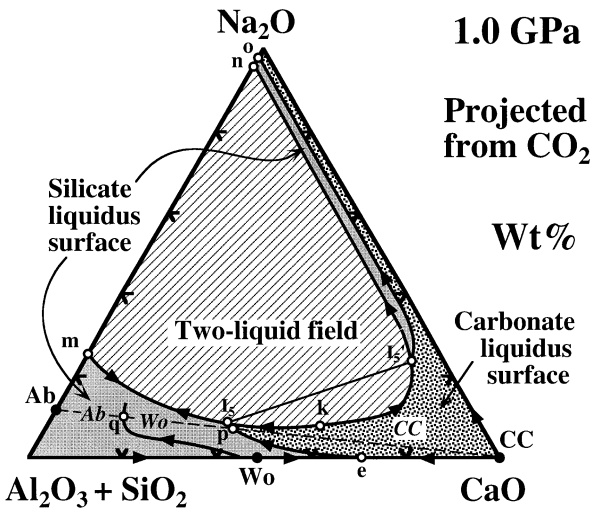

Fig. 2. Miscibility gap (two-liquid field), silicate liquidus surface, and carbonate liquidus surface at 1 GPa presented in the Hamilton projection, based on results intersected by the join Ab–CC at 1–2·5 GPa (after Lee & Wyllie, 1996, fig. 15b). Italic characters *Ab*, *Wo*, and *CC* indicate the liquidus fields for albite, wollastonite, and calcite. Liquidus piercing points p and q along Ab–CC were determined by Lee & Wyllie (1996), and the eutectic e between Wo and CC by Huang & Wyllie (1974). Curves e–p–I_5 and I_5'–o indicate the compositions of liquids which coprecipitate silicate and carbonate minerals with vapor. Curve m–I_5–k–I_5'–n delineates the limit of the miscibility gap where silicate- and carbonate-rich liquids coexist with a mineral and vapor. k is the critical point where Ls = Lc. I_5 and I_5' are pseudoternary isobaric invariant points for the assemblage Wo + CC + Ls + Lc + V.

the miscibility gap, but most subsequent studies presented the immiscible liquids corresponding to an isothermal miscibility gap. Lee & Wyllie (1992*a*, *b*, *c*) emphasized that the existence of a miscibility gap did not mean that all carbonatites were immiscible fractions. The liquidus paths followed by silicate–CO_2 magmas could (1) reach a miscibility gap, (2) reach a silicate–carbonate liquidus field boundary and coprecipitate silicates and carbonates, or (3) terminate at a eutectic precipitating silicates with evolution of CO_2 vapor. The results in Fig. 2 illustrate the tentative positions of the silicate–carbonate (e–p–I_5) and albite–wollastonite (through q) liquidus field boundaries. The new results in this contribution permit a more complete construction of silicate–silicate field boundaries in the liquidus volume between Ab–Ne–CC and ($Al_2O_3 + SiO_2$) in Fig. 1, providing additional constraints on the conditions leading to each of the three processes outlined above.

EXPERIMENTAL METHODS

The starting materials were: (1) primary standard grade $CaCO_3$ powders (Alfa Product), dried at 110°C for at least 1 day; (2) synthetic glass of 90 wt % $NaAlSiO_4$ and 10 wt % $NaAlSi_3O_8$ (prepared by Koster van Groos), dehydrated at 800°C for 4 h. Starting mixtures of these components were ground with ethanol in an agate mortar for 1 h. All starting mixtures (~5 mg for each run) were held for >1 h in a vacuum drying oven at 110°C before being loaded into platinum capsules ~4 mm long.

Experiments were undertaken using 1·27-cm diameter piston–cylinder apparatus, with calcium fluoride as a pressure medium. Temperature was controlled and monitored by a $W_{95}Rh_5$–$W_{74}Rh_{26}$ thermocouple with no correction for the effects of pressure on the e.m.f. Run duration varied from 1 to 12 h. Experiments were terminated by turning off the electrical power while the system remained near isobaric, and the quenching rate was ~100°C/s for the first 600°C. Pressure accuracy is about ±0·05 GPa, and temperature accuracy is estimated to be ±10°C. No pressure correction was made for the effects of friction.

Run products were mounted in a brass holder with petropoxy, polished by Al_2O_3 powders and cleaned by compressed air, without using water, and then carbon-coated. Phases were identified by textures and morphologies observed under the petrographic microscope and a Camscan scanning electron microscope fitted with an energy dispersive X-ray system (EDS). Phases were analyzed by EDS using a beam current of 0·1 nA as measured on brass.

EXPERIMENTAL RESULTS

On the basis of the runs listed in Table 1, the phase fields intersected by the composition join $Ne_{90}Ab_{10}$–CC at 1·0 GPa are shown in Fig. 3. The interpretations of phases and textures are illustrated by the examples in Fig. 4. The phases encountered include nepheline (Ne), anorthite (An), scapolite (Scap), melilite (Mel), calcite (CC), silicate-rich liquid (Ls), carbonate-rich liquid (Lc), and vapor (V). As minerals were precipitated during the quench, detailed study was required to interpret some of the phase assemblages. Representative compositions of immiscible silicate–carbonate liquid pairs are listed in Table 2 and illustrated in Fig. 5. The positions of dashed lines are uncertain, but they provide an internally consistent interpretation of the available data. The experiments were aimed at determination of the liquidus relationships, the piercing points on either side of the miscibility gap (P, Q), and the points separating different liquidus minerals (R, S, T). These points were determined partly on the basis of runs plotted in Fig. 3, and partly on tie-lines connecting measured liquid compositions (S, T, Fig. 5), with additional constraints required to complete the phase diagrams in Figs 6, 7 and 8. P and S are closely determined, and the possible error in Q and R is discussed below.

Table 1: Experimental results for the join $NaAlSiO_4$–$NaAlSi_3O_8$–$CaCO_3$

Run	Starting mixture (wt %)		Pressure (GPa)	Temperature (°C)	Time (h)	Interpreted phase assemblage
	Silicate	$CaCO_3$				
120	20	80	1·0	1300	2	Mel + Lc + V
121	20	80	1·0	1250	4	Scap + Mel + CC + Lc + V
122	20	80	1·0	1200	4	Ne + An + Mel + CC + Lc + V
117	40	60	1·0	1300	1·5	Ls + Lc + V
119	40	60	1·0	1250	2	An + Mel + Ls + Lc + V
149	40	60	1·0	1200	4	Ne + An + Lc + V
118	40	60	1·0	1150	4	Ne + An + CC + Lc + V
123	60	40	1·0	1250	2	Ls + Lc + V
148	60	40	1·0	1150	4	Ne + An + CC + Lc + V
130	70	30	1·0	1350	2·5	Ls + Lc + V
127	70	30	1·0	1300	2	Ls + Lc + V
128	80	20	1·0	1400	1	Ls + V
129	80	20	1·0	1350	2	Ls + Lc + V
145	80	20	1·0	1300	2	Ls + Lc + V
150	80	20	1·0	1250	4	Ne + Ls + Lc + V
131	90	10	1·0	1400	1	Ls + V
132	90	10	1·0	1350	2	Ne + Ls + V
144	90	10	1·0	1300	12	Ne + Ls + Lc + V
147	90	10	1·0	1300	6	Ne + Ls + Lc + V
146	90	10	1·0	1250	6	Ne + Ls + Lc + V

Starting silicate glass: 90 wt % $NaAlSiO_4$ + 10 wt % $NaAlSi_3O_8$. Ne, nepheline; An, anorthite; Scap, scapolite; Mel, melilite; CC, calcite; Ls, silicate-rich liquid; Lc, carbonate-rich liquid; V, vapor.

Table 2: Immiscible liquid compositions on a CO_2-free basis (wt %)

Run (SM)	Temp. (°C)	Phase (NA)	SiO_2	Al_2O_3	Na_2O	CaO
129 (20)	1350	Ls (3)	39·3	31·8	17·6	11·2
		Lc (3)	1·3	0·5	40·2	57·9
130 (30)	1350	Ls (3)	38·1	31·2	14·7	16·0
		Lc (3)	1·9	0·8	33·6	63·6
145 (20)	1300	Ls (2)	39·5	33·3	17·4	9·7
		Lc (1)	1·5	1·8	31·2	65·5
127 (30)	1300	Ls (2)	39·0	33·1	15·5	12·4
		Lc (3)	1·2	1·0	37·6	60·2
117 (60)	1300	Ls (3)	34·7	29·5	7·5	28·3
		Lc (3)	4·0	1·5	20·7	73·8
123 (40)	1250	Ls (2)	39·9	31·9	13·6	14·7
		Lc (3)	2·2	0·7	20·1	77·0
119 (60)	1250	Ls (3)	36·5	30·3	8·7	24·6
		Lc (3)	2·3	1·3	16·0	80·4

SM, starting mixture: 20–20 wt % calcite + 80 wt % silicate. NA, number of analyses (Fig. 5) used to calculate the mean composition of a phase (except for Lc in run 145). (See Fig. 5 for the range of individual measurements for each phase.)

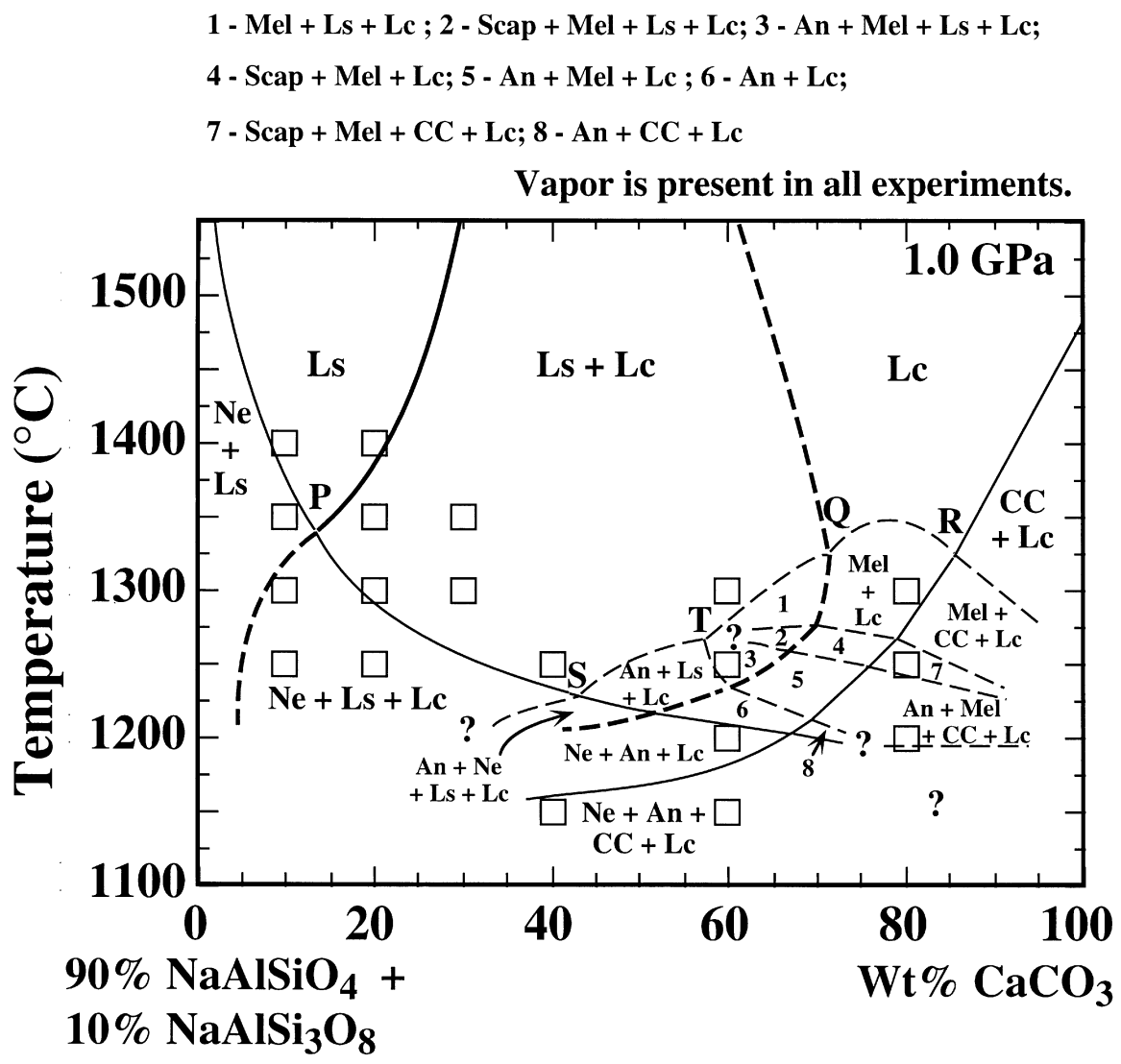

Fig. 3. Phase fields intersected by the join $Ne_{90}Ab_{10}$–CC at 1·0 GPa. Bold curves locate the fields for the existence of immiscible liquids Ls and Lc. Dashed curves indicate tentative determination of the phase field boundaries. Solidus is not determined. It should be noted that the dashed horizontal line near 1200°C indicates the appearance of an isobaric invariant assemblage: Ne + An + Mel + CC + Lc + V. Ne, nepheline; An, anorthite; Scap, scapolite; Mel, melilite; CC, calcite; Ls, silicate-rich liquid; Lc, carbonate-rich liquid. (See text for descriptions of the liquidus-piercing points P, Q, R, T and S.)

Phase fields intersected

The results from the experiments (open squares) plotted in Fig. 3 have been interpreted in terms of the phase boundaries and phase assemblages as shown. The presence of vapor is evident by the appearance of pore space on the top portion of a capsule, and bubbles trapped in quenched liquids; however, complex quench textures in some lower-temperature experiments (e.g. 148 and 118 at 1150°C) made positive identification of vapor difficult.

Liquid was produced in all experiments, and quenched to a variety of textures depending on composition and run temperature. The solidus was not determined. Silicate-rich liquids at higher temperatures usually quenched to a glass (Fig. 4a), but at lower temperatures the glass contained quench nepheline (Fig. 4b). Carbonate-rich liquids always formed calcite dendrites (~several μm; Fig. 4b–d), with nyerereite and thin lamellae of silicate-rich material (Fig. 4f).

The upper-temperature stability limits for calcite and nepheline are fairly well defined (Fig. 3, continuous lines). The melting temperature of calcite at 1 GPa is 1480°C (Irving & Wyllie, 1975). Neither the fusion temperature

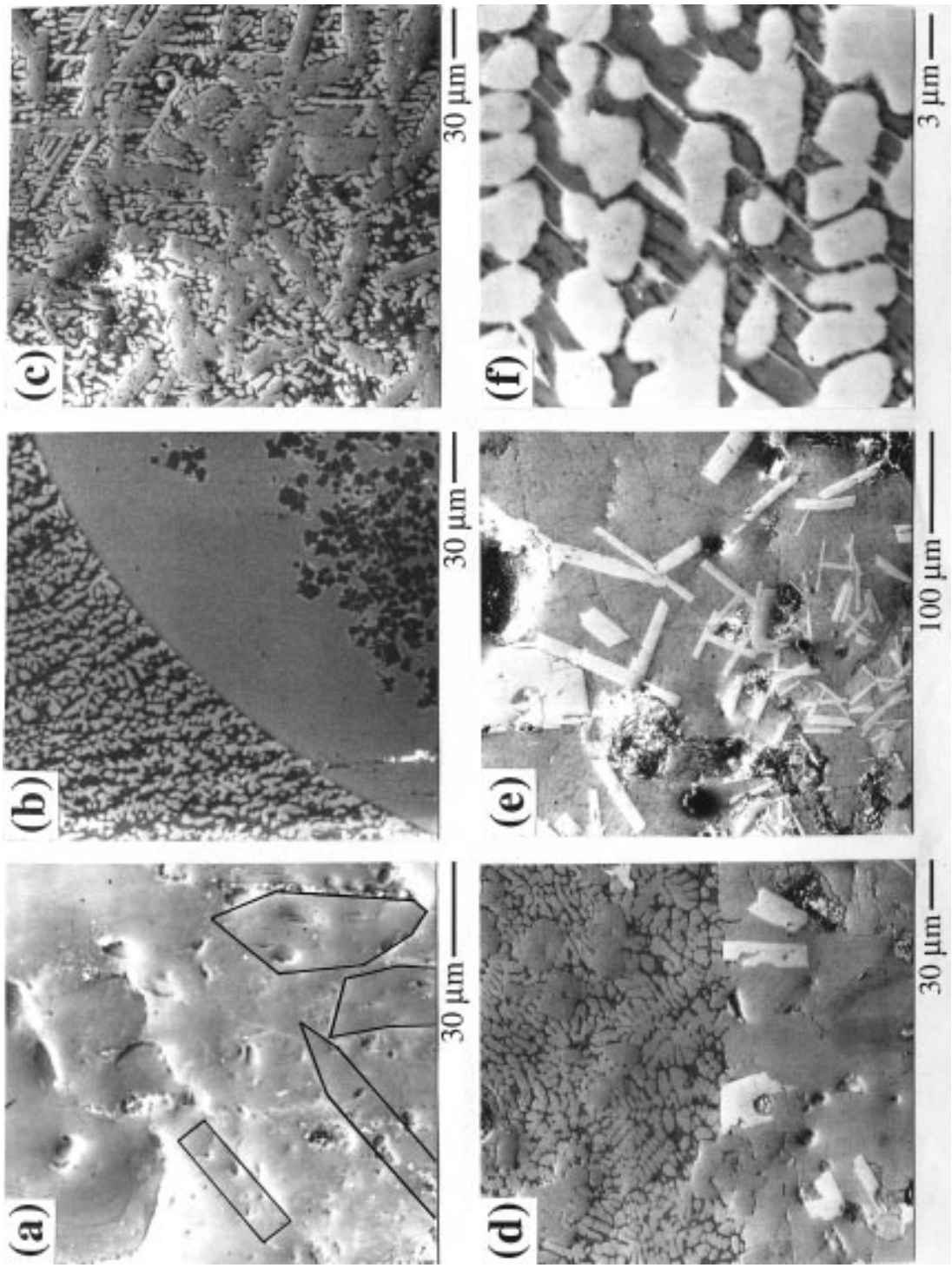

Fig. 4. Back-scattered electron photomicrographs showing the experimental phases (Table 1). (a) Primary nepheline (the outlined crystals) set in glassy matrix, with intersitial quench nepheline not discernible in the image (run 132). (b) Quenched immiscible silicate-rich liquid with dark quench nepheline crystals, surrounded by quenched carbonate-rich liquid of dendritic texture (run 123). (c) Elongated anorthite (intermediate gray) set in quenched carbonate-rich liquid (run 149). Nepheline also occurred, but is not distinguishable in the picture from the dark quench nyerereite. (d) Scapolite (~30 µm, near-rectangular crystals) enclosed in quenched carbonate-rich liquid (dendritic texture) and in the lower calcite layer (massive material; scapolite not discernible). Melilite appears as the lightest colored crystals (run 121). (e) Melilite laths (light color) with quenched carbonate-rich liquid (run 120). (f) Enlarged view of quenched carbonate-rich liquid, including calcite dendrites (light, rounded), interstitial nyerereite (dark), and silicate-rich lamellae (palest; run 119).

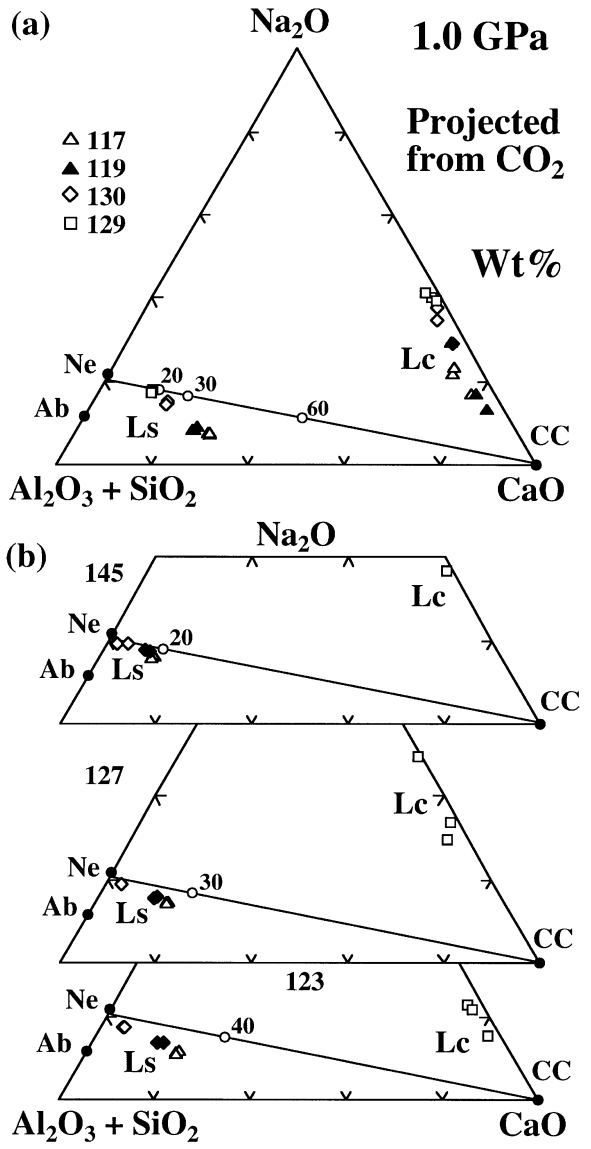

Fig. 5. (a) Individual analyses for the immiscible liquids from runs 117, 119, 130 and 129. ○, relevant starting mixtures (60 wt % CC for 117 and 119, 30 wt % for 130, and 20 wt % for 129). Silicate-rich liquids (near Ls) quenched to a uniform glass, whereas carbonate-rich liquids (Lc) quenched to calcite dendrites with nyerereite, showing large heterogeneity in composition. (b) Measurements of the two-liquid compositions in runs 123, 127 and 145. Silicate-rich liquids quenched to glass (△) with nepheline (◇); analyses including both portions are considered to represent the actual liquid compositions (◆).

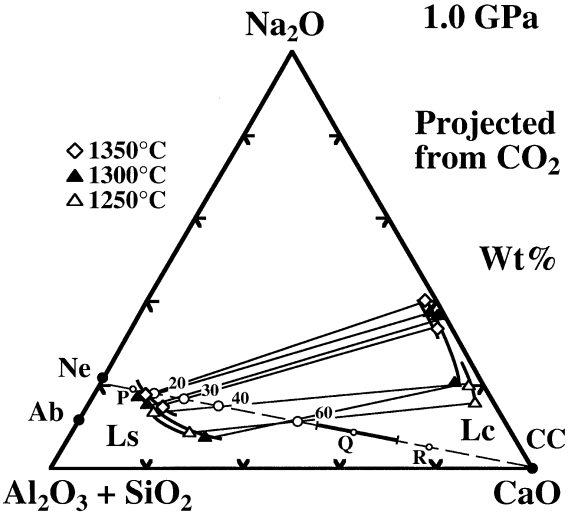

Fig. 6. Average two-liquid compositions (Table 2) with corresponding tie-lines, including results at 1350°C (runs 130 and 129), 1300°C (117, 127 and 145), and 1250°C (119 and 123). Three pairs of two-liquid isotherms are drawn passing through the data, with those at lower temperature showing wider separation. The positions of piercing points P, Q (with error bar), and R along the join $Ne_{90}Ab_{10}$–CC are also indicated.

of nepheline nor the melting relationships of the join $NaAlSiO_4$–$NaAlSi_3O_8$ have been determined experimentally at 1 GPa. The congruent melting temperature of $Ne_{90}Ab_{10}$ in Fig. 3 is estimated to be ~1620°C, using published 1 atm data (Greig & Barth, 1938) extrapolated by 110°C corresponding to the pressure increase [for pure $NaAlSi_3O_8$ as determined by Boyd & England (1963); see also Bell & Roseboom (1965)].

The bold lines (Fig. 3, solid and dashed) bounding the miscibility gap are based on the runs and on analyses of coexisting quenched liquids. The slope of the silicate-rich limb above 1400°C is arbitrarily drawn, roughly extended from the section below 1400°C to point P. The carbonate-rich limb above Q is sketched with a negative slope symmetric to the silicate-rich counterpart, reflecting that the size of the hyper-liquidus miscibility gap decreases with increasing temperature (e.g. Freestone & Hamilton, 1980; Lee & Wyllie, 1996). There is no evidence for immiscible liquids in runs at 1200°C and below, indicating that the boundary of the miscibility gap closes with decreasing temperature, as indicated by the bold dashed line swinging towards the Ne-rich direction at lower temperatures (between runs 119 and 149, Table 1).

The crystallization of melilite, anorthite, scapolite, calcite and nepheline at lower temperatures (<1300°C) in the $CaCO_3$ half of the join indicates complex phase relationships (Fig. 3). The compositions of melilite, scapolite, and anorthite are close to their ideal compositions (Geh, Scap, and An, respectively, in Fig. 1). Melilite commonly formed large prismatic crystals (lightest color crystals, Fig. 4d and e) with sizes up to 100×30 μm^2, and contained a few percent of Na_2O, representing solid solution toward soda melilite. Run 121 was the only experiment containing scapolite, commonly with inclusions of carbonate-rich melt, occurring as rectangular crystals up to 30 μm in the layer of quenched carbonate-rich liquid (Fig. 4d). Anorthite formed elongated crystals

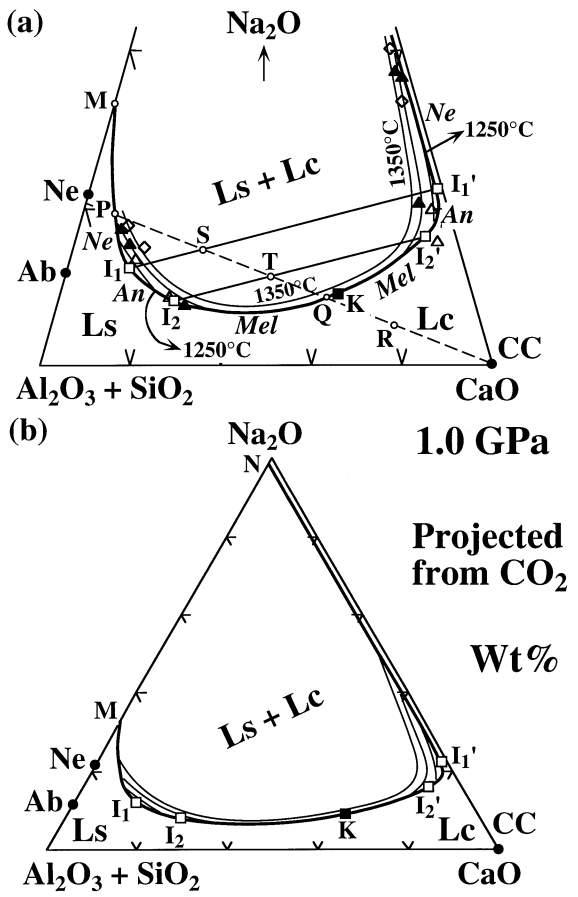

Fig. 7. (a) Lower portion of the Hamilton projection (Fig. 6; vertical exaggeration of two), showing the miscibility gap field boundary (bold curve) through P, I_1, I_2, Q, K, I_2' and I_1', two-liquid isotherms at 1350, 1300 and 1250°C, and tie-lines I_1–I_1' and I_2–I_2' intersecting the studied join at S and T (see text). Italic characters *Ne*, *An* and *Mel* surrounding the field boundary indicate the liquidus fields for nepheline, anorthite and melilite. (b) Complete range of the field boundary to proper scale.

(up to 30 μm in length) within carbonate-rich liquids, or intergrown with nepheline, calcite or melilite (Fig. 4c and d).

The composition join intersects a series of piercing points for liquidus field boundaries: P between the liquidus surfaces for nepheline and silicate-rich immiscible liquid (Ls); Q between carbonate-rich immiscible liquid (Lc) and melilite; and R between melilite and calcite. Points S and T within the miscibility gap are closely defined, as discussed below in connection with Figs 6 and 7a.

The nepheline liquidus drops steeply as $CaCO_3$ is added, down to the piercing point P (1335°C and 14 wt % CC), where it is joined by immiscible carbonate-rich liquid. Figure 4a illustrates unambiguous primary nepheline (outlined) from run 132, which forms large crystal prisms up to 50×20 μm^2; however, nepheline produced below 1200°C is generally smaller (~10 μm). There are also some minute crystals of nepheline (several μm across) near the large nepheline, not discernible in the picture. Nepheline contains variable amounts of CaO which increase with changing bulk composition towards $CaCO_3$, from <1 wt % to ~6 wt % CaO. Nepheline compositions project onto the line between Ne and An in Fig. 1, suggesting solid solutions dominantly with anorthite. Bowen (1912) reported that at 1 atm nepheline could dissolve as much as 35 wt % anorthite, with CaO equivalent to 7 wt %.

The calcite liquidus also drops steeply to piercing point R for the calcite–melilite field boundary (near 1325°C, 85 wt % $CaCO_3$). Calcite in this join always formed a distinct layer at the lower portion of a charge, as shown in Fig. 4d, and was commonly intergrown with nepheline, melilite or anorthite. The calcite crystals exhibited a hexagonal habit, in contrast with the rounded calcite crystals reported in many silicate–carbonate systems (see Huang *et al.*, 1980; Lee *et al.*, 1994). The calcite-precipitating fields are first intersected by the melilite liquidus at R, then joined by scapolite, anorthite, and finally nepheline at 1200°C and below. Contrary to the results in the join Ab–CC (Lee & Wyllie, 1992*a*, *b*, 1996), the calcite liquidus here does not intersect the two-liquid field.

The melilite liquidus is intersected in a narrow compositional range between the miscibility gap and the calcite liquidus, Q to R, and completion of the phase diagram in Figs 6, 7 and 8 shows that the melilite-out boundary (Fig. 3) extends between the calcite liquidus (R) and the defined point T (Figs 3 and 7a) within the miscibility gap (compare runs 117 and 119). The errors associated with the location of points Q and R will be considered in connection with Fig. 7. Melilite becomes unstable below the fields 3 and 5 (compare runs 119 and 149). The fields 2, 4, and 7 in Fig. 3 indicate a small temperature interval where scapolite may be stable (assumed to cover a compositional range similar to that of the melilite-out boundary). Below this interval the phase assemblages are joined by anorthite through a wide compositional range. The scapolite–anorthite temperature relationship is consistent with the results of Goldsmith & Newton (1978), and we assume the field boundary between the two stability fields to be a carbonation–decarbonation relation. It should be noted that between the Lc limb of the miscibility gap (dashed bold curve below Q) and the calcite field boundaries (continuous curve below R) are fields where carbonate-rich liquids precipitate assemblages of silicate minerals, joined by calcite at lower temperatures.

Compositions of immiscible liquids

The compositions of seven pairs of immiscible liquids for the temperature interval 1250–1350°C are listed in Table

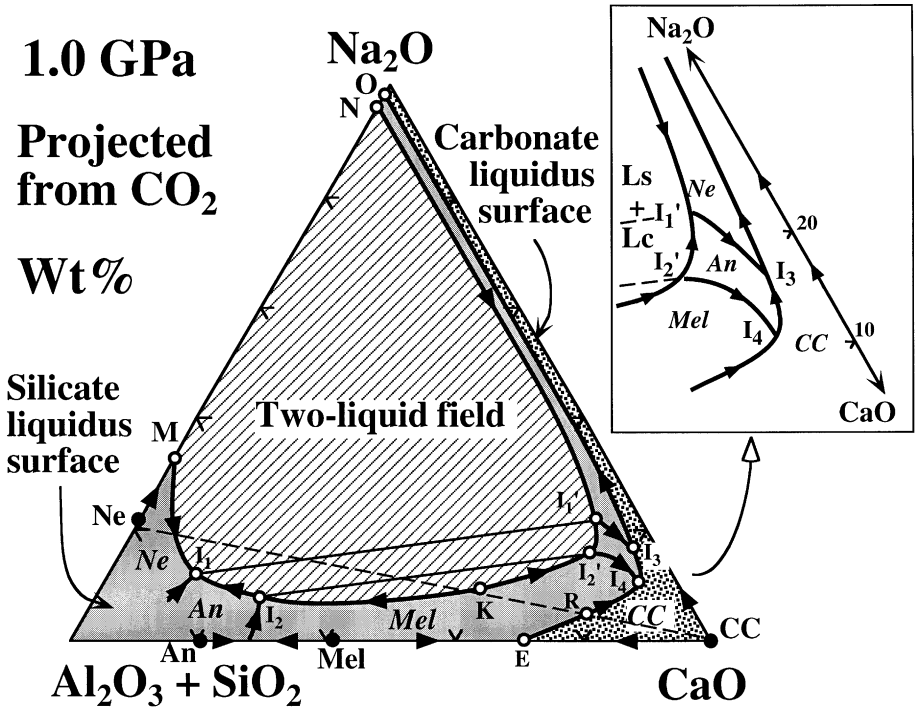

Fig. 8. Completed liquidus field boundary diagram based on Fig. 3, and Figs 5–7, showing the miscibility gap, and the silicate and carbonate liquidus surfaces (compare Fig. 2). The key boundaries, cooling directions, and pseudoternary isobaric invariant points are also indicated (see text). The details near the CaO corner of the projection are sketched in the upper-right inset. It should be noted that the compositions of Ne, An, and Mel (●) are ideal values (e.g. Ne, An, and Geh, Fig. 1).

2. One of these experiments, 119, contains in addition small amounts of melilite and anorthite. Figures 5 and 6 show the liquid compositions in the Hamilton projection (Fig. 1b), with compositions recalculated as CO_2 free. The open circles labeled 20, 30, 40, 60 correspond to the projected starting mixtures from Fig. 3 with 20 wt % $CaCO_3$, etc. It should be noted that the mixture '30' contains ~20 wt % CaO, and mixture '60' contains ~45 wt % CaO in the projection. The compositions of phase boundaries and piercing points in Fig. 3 show liquid compositions in terms of wt % $CaCO_3$, but the projected analyses in Figs 5 and 6 show instead wt % CaO, consistently lower than the wt % $CaCO_3$. The actual carbonate compositions (wt %) remain unknown without measurements of the CO_2 content of pre-quench liquids. The presence of vapor in all runs shows that the liquids in Fig. 3 contain less CO_2 than indicated by the wt % $CaCO_3$ in the starting mixtures.

Lee *et al.* (1994) determined the CO_2 solubilities in parts of the system CaO–SiO_2–CO_2. The position of the CO_2-saturated liquidus provides an indication of the actual liquid composition. The geometrical relationship between a CO_2-saturated liquidus surface and the Hamilton projection of Figs 5 and 6 was illustrated by Lee & Wyllie (1996, figs 13 and 14). Carbonate-rich liquids in Figs 5 and 6 contain an amount of carbonates slightly below the values indicated on the starting join silicate–$CaCO_3$, but liquids near Q and toward the silicate components become substantially lower in carbonate contents compared with the silicate–$CaCO_3$ join, being located between the join and the CO_2-free silicate–CaO projection.

Runs 117, 119, 129, and 130 (Table 1, Fig. 3) yielded silicate glass, and runs 123, 127, and 145 (Table 1, Fig. 3) contained silicate glass with quench nepheline. Individual analyses for the quenched silicate- and carbonate-rich liquids from the first four runs are plotted in Fig. 5a, and from the other three in Fig. 5b. Averages of these analyses (2–3 measurements for each quenched liquid except one for Lc of run 145) are plotted in Fig. 6 and connected by tie-lines, and grouped in terms of temperature.

Figure 5a shows three analyses for each liquid in four runs. The silicate analyses cluster closely, but the

carbonate analyses show a wider spread. The quench products of carbonate-rich liquids show large heterogeneity in calcite–nyerereite distribution (e.g. Fig. 4b, 4f). Areas up to 100 μm^2 were analyzed by the EDS method, but the areas suitable for the rastering mode were still too small to compensate for the heterogeneity; the variation in analyses trends generally subparallel to the $CaO–Na_2O$ side of the projection. A line connecting each pair of average coexisting liquid compositions would pass very close to the corresponding starting mixture, as shown in Fig. 6. This is true even for run 119, which contains some melilite and anorthite.

Figure 5b shows similar analyses from the three runs with quench nepheline in the glass. For the silicate liquid in each run, three types of analyses are plotted: the open diamonds near Ne give compositions for quench nepheline crystals; the open triangles are for the mineral-free glass; the filled diamonds are for larger areas (>1000 μm^2) including both glass and quench nepheline. The latter analyses represent the original liquid composition, lying between the open diamonds and the squares as they should. The analyses of carbonate-rich liquids in Fig. 5b have a similar spread, and similar relationship to the silicate liquids as in Fig. 5a, although the range for run 127 is somewhat wider. Only one rastered analysis is given for run 145, covering ~1000 μm^2 area.

The average analyses for the seven pairs of coexisting liquids, connected by tie-lines and identified in terms of temperatures, are plotted together in Fig. 6. A noteworthy feature is how closely the tie-lines pass through the starting compositions. The tie-lines are subparallel at all temperatures within the narrow interval 1250–1350°C, with a regular arrangement of the two-phase tie-lines as a function of changing bulk composition (including run 119 for composition '60' at 1250°C containing some melilite and anorthite). The only exception is run 117 at 1300°C for mixture '60'. The rotation of the tie-line for 117 compared with the others could conceivably be a temperature effect between 117 (1300°C) and 119 (1250°C) enhanced as the immiscible liquids approach closure.

Small differences are distinguishable as a function of temperature. The short arcs connect analyses of quenched liquids at the three temperatures 1350°C, 1300°C and 1250°C, and thus represent portions of isotherms on the liquidus surface of the miscibility gap, which becomes larger with decreasing temperature. The data points overlap, but the isotherms must be separate, as drawn. These partial isotherms, along with other definitive points from Fig. 3, permit construction of part of the liquidus surfaces and field boundaries intersected by the composition join $Ne_{90}Ab_{10}$–CC.

Additional liquid compositions are given by the points P, Q and R from Fig. 3. These represent liquids for piercing points on liquidus field boundaries. P is closely bracketed at 14 wt % $CaCO_3$. The calcite-out phase boundary is closely defined, so the position of R depends on the temperature of the melilite liquidus, which occurs above 1300°C (run 120). The piercing point R must lie at a cotectic temperature minimum between the liquidus fields for calcite and melilite (Fig. 8), requiring a temperature maximum on the melilite liquidus between R and Q/T. We have assumed a maximum temperature of ~1350°C for the melilite liquidus. This provides a cross-section with the calcite liquidus dropping through more than 150°C to reach the calcite–silicate field boundary at R, which is consistent with several other calcite–silicate joins at several pressures (e.g. Maaloe & Wyllie, 1975; Huang *et al.*, 1980; Lee & Wyllie, 1996). Given the steep liquidus surface for calcite, we conclude that the point R is close to 85 wt % $CaCO_3$, with possible error of ± 3 wt % $CaCO_3$. The composition of Q in Fig. 3 is bracketed only between 60 wt % and 80 wt % $CaCO_3$, but it is also constrained because the 1300°C isotherm in Fig. 6 must pass very close to Q. We place the position of Q at 72 ± 8 wt % $CaCO_3$, as indicated for its projected position Q in Fig. 6. Despite the uncertainties in Q and R, their relative positions in the phase diagram cannot be changed, and hence the corresponding petrological conclusions remain unaffected by the errors.

P, Q and R are plotted at 8 wt %, 59 wt % and 76 wt % CaO, respectively, in the CO_2-free projection in Fig. 6. As discussed above, the actual liquids are situated between the Fig. 3 join and the CO_2-free projection.

MISCIBILITY GAP AND LIQUIDUS FIELD BOUNDARIES IN THE SYSTEM $Na_2O–CaO–Al_2O_3–SiO_2–CO_2$

The experimental data obtained from the join Ab–$CaCO_3$ (Lee & Wyllie, 1996) were presented in the Hamilton projection (Fig. 1b) as pseudoternary phase relationships (Fig. 2). Similarly, the new near-liquidus experimental data obtained from the join $Ne_{90}Ab_{10}$–$CaCO_3$ can be treated as pseudoternary in projection, because the immiscible liquid compositions (molecular Al/Si of silicate-rich liquids ~0·95; Table 2) are very close to the triangular slice $CaO–Na_2O–Ne_{90}Ab_{10}$ (Al/Si = 0·9) extending through the excess-CO_2 tetrahedron (Fig. 1). The data in Figs 3 and 6 are first combined to define the miscibility gap and liquidus field boundaries around it, along with the primary minerals along the field boundaries (Fig. 7). Sequences of crystallization illustrated in Fig. 3 are then combined with published or inferred data on bounding systems to begin mapping out the field boundaries separating primary phase fields for the CO_2-saturated silicate and carbonate liquidus surfaces (Fig. 8).

The pseudoternary system through $Ne_{90}Ab_{10}$–$CaCO_3$–Na_2CO_3

The experimental data on phase fields (Fig. 3) and liquid compositions (Figs 5 and 6) permit construction of parts of the vapor-saturated liquidus surface for the miscibility gap, bounded by the field boundaries for two immiscible liquids Ls + Lc coexisting with one mineral and vapor. Figure 7a with vertical exaggeration of two shows the data sources and construction methods, and Fig. 7b shows the projected CO_2-free results to scale. Points P (1335°C) and Q (1325°C) are on the miscibility gap field boundary, coexisting with nepheline and melilite, respectively (Figs 3 and 6). The bold continuous line through P and Q is our estimate of the position of the field boundary enclosing the miscibility gap, similar to the topology in Fig. 2, with justification following. The silicate side of the field boundary is extended to terminate arbitrarily on the Ne–Na_2O side at M, based on previous results in the Ca-free system from Koster van Groos & Wyllie (1966, 1973) and Kjarsgaard & Hamilton (1988, 1989) (see Lee & Wyllie, 1996; Figs 2 and 8), and the carbonate side is extended to show a narrow field for carbonate-rich liquids extending from CaO to Na_2O (Lee & Wyllie, 1996; Figs 2 and 8).

The isotherms for the miscibility gap liquidus given in Fig. 6 are more or less concentric with the limiting field boundary, terminating on it, or remaining within it, and fitted with the temperatures of P and Q, as well as with the temperatures of the additional tie-lines shown passing through S and T. Nepheline and melilite are the primary minerals on the silicate liquidus surface between P and Ne, and between Q and R, respectively, and calcite (R–CaO) is the primary mineral on the carbonate liquidus surface (Figs 3 and 7).

Figure 3 shows anorthite on the liquidus between nepheline and melilite (S–T). The anorthite liquidus is therefore adjacent to the field boundary between the two pairs of pseudoternary isobaric invariant points I_1–I_2, and I_1'–I_2' (open squares) in Fig. 7. The tie-lines I_1–I_1' and I_2–I_2' must pass through the points S and T (Fig. 3), as shown in Fig. 7. The corresponding phase assemblages are I_1–S–I_1' (1230°C): Ne + An + Ls + Lc + V; and I_2–T–I_2' (1270°C): An + Mel + Ls + Lc + V. The precise positions of these six points are uncertain, but the constraints are fairly close. The error bars in terms of composition and temperature are within our normal brackets of 10 wt % $CaCO_3$ and 50°C. The tie-lines must be approximately parallel to the other tie-lines (Fig. 6). Given these constraints, there is little variation possible for the positions of I_1, I_1', I_2, I_2', S and T. The positions of S and T in Fig. 3 are drawn to correspond to the points constructed in Fig. 7.

The estimated invariant points I_1, I_2, I_2' and I_1' provide temperature constraints for the terminations of liquidus isotherms on the miscibility gap. They also define the limits for the liquidus minerals nepheline, anorthite, melilite, anorthite, and nepheline. It should be noted that the primary mineral on the miscibility gap field boundary for carbonate-rich liquids from I_1' to near Na_2O is nepheline, not a carbonate [see Fig. 2 boundary I_5'–n, and Lee & Wyllie (1996), boundaries G–N and g–n in fig. 15]. Carbonate is precipitated along with the silicate at lower temperatures, as indicated by the mineral sequences in the right-hand side of Fig. 3 [see Fig. 2 boundary I_5'–o, and Lee & Wyllie (1996), boundaries G–O and g–o in fig. 15].

There must be a critical point where Ls = Lc on the miscibility gap field boundary between I_2 and I_2', associated with the liquidus for melilite. The distribution of isotherms in Fig. 7 indicates that this is also a temperature maximum, which is consistent with the tentative dashed lines in Fig. 3. We have estimated K near Q, at temperature near 1330°C.

Figure 8 shows the completed pseudoternary phase diagram, analogous with Fig. 2, showing the three major features, the miscibility gap (line-shaded two-liquid field), the silicate liquidus surface (gray), and the carbonate liquidus surface (dotted). The miscibility gap is defined by the liquidus field boundaries and pseudoternary isobaric invariant points transferred from Fig. 7: M–I_1–I_2–K–I_2'–I_1'–N. The region near the CaO–Na_2O side of the projection (I_1' and I_2') is distorted compared with Fig. 7, to show some details for the carbonate-rich liquids. The primary liquidus minerals nepheline, anorthite, and melilite, on the silicate-rich field boundary M–K, must be repeated along the carbonate-rich field boundary K–N. Therefore, no primary carbonate mineral can be precipitated from the carbonate-rich liquids, Lc, which remain in equilibrium with the silicate-rich liquids, Ls. Crystallization directions along parts of the boundaries are indicated by arrows.

On the silicate liquidus surface, several curves are sketched for the field boundaries between Ne and An, and between An and Mel. For the silicate-rich liquids, the curves are largely schematic, starting at somewhat arbitrary eutectics in the joins Ne–An and An–Mel, and terminating at the better-constrained points I_1–I_1' and I_2–I_2'. For the carbonate-rich liquids (see the enlarged inset diagram), two field boundaries are defined between I_1' and I_3, and I_2' and I_4, respectively, where I_3 and I_4 are pseudoternary isobaric invariant points for Ne + An + CC + Lc + V and An + Mel + CC + Lc + V. Points I_3 and I_4 are plotted close to the measured compositions of carbonate-rich liquids in runs 148 and 121 with similar phase assemblages (Table 1, Fig. 3). The arrangement of field boundaries and arrows in Fig. 8 (inset) is consistent with the sequences of crystallization observed for liquids with compositions between Q and R in Fig. 3, neglecting the complication of possible

primary scapolite (phase fields 2, 4 and 7 in Fig. 3). There is probably a thermal divide on the melilite liquidus surface extending from the temperature maximum at critical point K.

The silicate–carbonate liquidus field boundary starts from a postulated eutectic E between Mel and CC on the ($Al_2O_3 + SiO_2$)–CaO baseline (compare e in Fig. 2), passes through the estimated piercing point R (Figs 3 and 6), and then passes through the deduced pseudoperitectic points I_4 and I_3 where melilite is successively replaced by anorthite and nepheline. It then extends to O as discussed above (compare Fig. 2). The carbonate liquidus surface is thus restricted to a field with primary calcite near CaO, which extends along a narrow area close to the side CaO–Na_2O, with decreasing temperature. The primary liquidus carbonate minerals involved change from calcite to alkali-rich carbonates (e.g. nyerereite, sodium carbonate), as indicated by the classic study of Cooper *et al.* (1975) at lower pressures.

The pseudoternary systems through $Ne_{90}Ab_{10}$–$CaCO_3$–Na_2CO_3 and Ab–$CaCO_3$–Na_2CO_3

The two pseudoternary isobaric phase diagrams for the triangular slices CaO–Na_2O–silicate through Fig. 1a which include $Ne_{90}Ab_{10}$ (Fig. 8) and Ab (Fig. 2) intersect the same major liquidus fields (the silicate–carbonate miscibility gap, silicate and carbonate liquidus surfaces), but with some significant differences. The key features of Figs 2 and 8 are compared in Fig. 9, which shows the lower parts of the diagrams with vertical exaggeration of two. In Figs 8 and 9a, the silicate–carbonate liquidus field boundary does not intersect the miscibility gap field boundary, and the miscibility gap is therefore surrounded by the liquidus surface for primary silicates. In Figs 2 and 9b, the silicate–carbonate liquidus field boundary does intersect the miscibility gap field boundary, bringing the carbonate liquidus surface into contact with the miscibility gap between the isobaric pseudoinvariant points I_5 and I_5'.

The liquidus surfaces for silicates involve different minerals and field boundaries, as expected given silicate end-members which are nepheline-normative (Figs 8 and 9a), or albite-normative (Figs 2 and 9b). In Fig. 9b, the albite–wollastonite field boundary has been extended through the determined point q (Fig. 2) to an estimated invariant point I_6 on the miscibility gap field boundary, which requires another tie-line I_6–I_6' for the pseudoinvariant phase assemblage Ab + Wo + Ls + Lc + V. The slope of the tie-line is comparable with those defined by the alkali-rich two-liquid pairs in Kjarsgaard & Hamilton (1989).

The compositional differences between the two experimental joins have been noted with respect to Fig. 1a, and the triangular slices drawn in Fig. 10a show the difference clearly in terms of Al_2O_3/SiO_2. The CO_2-free projected phase relationships intersected by the tetrahedron may be treated as pseudoquaternary. The $Ne_{90}Ab_{10}$–CC–NC plane has Al/Si = 0·9, and the Ab–CC–NC plane has Al/Si = 0·33. Curves A and B on these two planes in Fig. 10a are the miscibility gap field boundaries from Figs 2, 8, and 9 along with the isobaric pseudoinvariant points and the critical points, K and k, from Fig. 9. The immiscible liquid projections A and B, the field boundaries in Figs 2 and 8, then correspond closely to the curves of intersection of the miscibility gap with the two planes. The possible range of the miscibility gap is extrapolated down to the Al-free basal triangle SiO_2–CaO–Na_2O (Qz–CC–NC), and denoted by curve C. It is, however, difficult to extrapolate further towards the Al-rich region, and this part of the miscibility gap remains unplotted.

The three curves A, B and C from Fig. 10a provide the framework for the shaded surface of the miscibility gap in Fig. 10b (curves A and B are dashed lines). The pseudoternary isobaric invariant points on the triangular slices in Fig. 10a are located on the miscibility gap field boundaries traversing the shaded surface, as shown in Fig 10b. The field boundaries meet in pseudoquaternary isobaric invariant points for assemblages of two liquids, three minerals, and vapor, such as Plag + Wo + Mel + Ls + Lc + V at I_7 (open circle). The critical curve through K–k is the locus of critical liquids where Ls = Lc, dividing the miscibility gap liquidus surface into consolute liquids Ls occupying a large area to the left, and Lc to the right concentrated near the CaO corner of the tetrahedron and the axis CaO–Na_2O, with maximum 75–80 wt % CaO (Figs 2 and 8). This corresponds to no more than ~80 wt % dissolved $CaCO_3$ (assuming all CaO and Na_2O assigned to carbonate; see Lee & Wyllie, 1996). It should be noted in Fig. 8 that the liquidus field boundary for coprecipitation of melilite and calcite without liquid immiscibility can yield a liquid with ~85 wt % CaO (near I_4), or at most ~86 wt % $CaCO_3$. The consolute liquids Ls and Lc do not correspond to liquidus surfaces with primary minerals silicates and carbonates, respectively. Liquidus fields for both silicates and carbonates occur on both sides of the critical curve, Ls = Lc. This feature was emphasized by Lee & Wyllie (1996) in connection with the position of k and the silicate and carbonate liquidus surfaces in Fig. 2.

The field boundaries sketched in Fig. 10b connect the determined points, and locate the liquidus fields for immiscible liquids coexisting with nepheline, plagioclase, melilite, wollastonite or calcite. The area 'Plag' indicates the field of two liquids with plagioclase changing composition continuously from anorthite to albite as the bulk

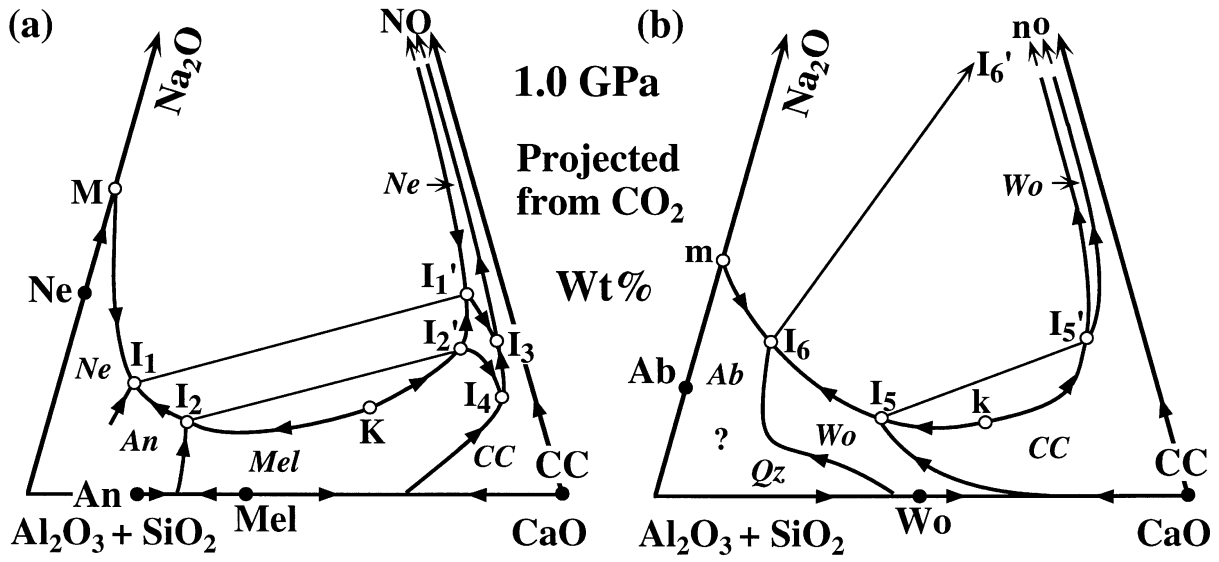

Fig. 9. (a) and (b), comparison of the lower portions of phase diagrams in Figs 2 and 8 (vertical exaggeration of two). The Ab–Wo liquidus field boundary in (b) now extends to the miscibility gap at I_6, with the corresponding immiscible carbonate-rich liquid I_6' (exact position not shown) along the section I_5'–n.

composition progresses from Ne–CC–NC to Ab–CC–NC. There is an additional field boundary for wollastonite and melilite coexisting with immiscible liquids and vapor, and this probably terminates at the invariant eutectic point I_7; the immiscible carbonate-rich liquid I_7' is alkalic, bracketed by the compositions of the carbonate-rich liquids I_2' and I_6' in Fig. 9a and b. A field for primary wollastonite is shown extending from I_7 between calcite and melilite around to the rear side of the miscibility gap; in an alternative arrangement the wollastonite field could terminate at another invariant point I_8, between I_5 and (K–k), for the assemblage Mel + Wo + CC + Ls + Lc + V; this would be reflected in a corresponding point I_8' on the carbonate side of the miscibility gap. All field boundaries and isobaric invariant points shown on the shaded surface for Ls are repeated on the liquidus surface for Lc, which is largely obscured by the miscibility gap (see Fig. 9 for the corresponding points).

Figure 11 summarizes the main pseudoquaternary phase relationships based on the two pseudoternary diagrams, with possible cooling directions indicated on some of the field boundaries. The light-shaded surface for the miscibility gap is reproduced from Fig. 10b, and a sketch of the silicate–carbonate liquidus field boundary surface (dark-shaded) is based on Figs 2, 8, and 9. These two surfaces meet in the wollastonite–calcite field boundary on the miscibility gap surface (Fig. 10b). The silicate–carbonate coprecipitation surface separates the large volume for primary silicates from the smaller volume for primary carbonates. The geometry of the rear part of the silicate–carbonate liquidus surface cannot be shown in Fig. 11, because the miscibility gap is in the way, and the part of the surface above the intersection (K–k)–I_5' obscures the part of the surface which swings around from the CaO corner and along the CaO–Na_2O side. The 3-D shape of the calcite volume, and its separation from the miscibility gap, can be visualized by comparing Fig. 11 with the 2-D slices showing intersections of the same surface and the calcite field in Fig. 9a and b.

The silicate–carbonate liquidus surface intersects the miscibility gap in the Ab join, but not in the Ne join (Fig. 9). Thus, increasing Al/Si is associated with separation of the surface from the miscibility gap. The intersection is shown between I_5 and I_5' in Figs 9b and 10, where calcite coexists with immiscible liquids. As bulk composition changes in the direction of increasing Al/Si (from the Ab join toward the Ne join), the length of the intersection (along the field boundary for CC + Ls + Lc + V, Fig. 9b) is reduced as I_5 and I_5' migrate toward the critical point k. For the composition with slightly higher Al/Si than that where I_5 and I_5' become coincident on the critical curve, the silicate–carbonate liquidus surface becomes separated from the miscibility gap, and carbonates do not coexist with the immiscible liquids, which is the situation in Fig. 9a.

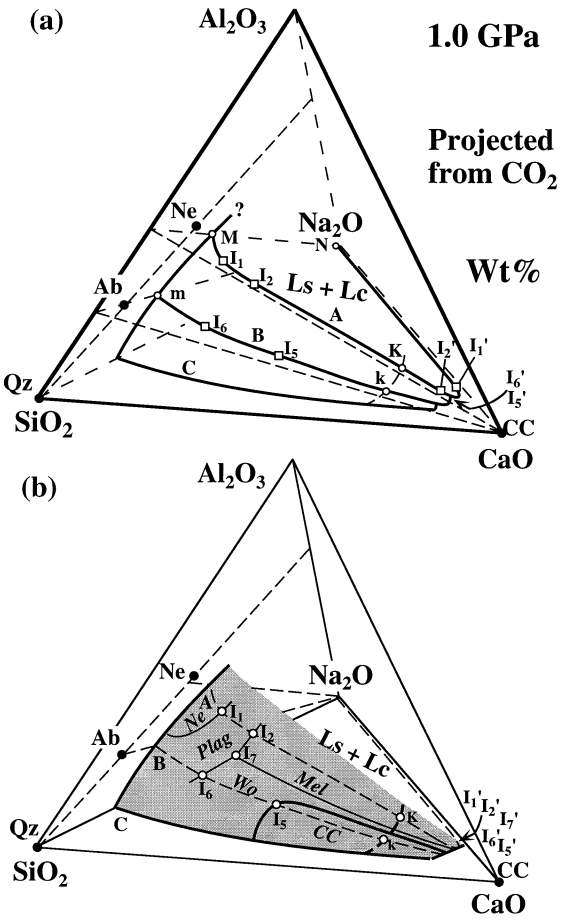

Fig. 10. (a) CO_2-saturated, compositional tetrahedron (Fig. 1a), showing the miscibility gap field boundaries of Figs 8 and 2 in space (curves A and B near the planes Ne–CC–NC and Ab–CC–NC). The miscibility gap field boundary C on the base of the tetrahedron is extrapolated from A and B. K–k indicates the critical curve for Ls = Lc. (b) Same projection as in (a), showing the surface of the miscibility gap (shaded area) with five-phase field boundaries (two liquids, two minerals, and vapor). Italic characters *Ne*, *Plag*, *Mel*, *Wo*, and *CC* on the surface mark the fields for nepheline, plagioclase (Ab to An), melilite, wollastonite, and calcite, coexisting with immiscible liquids (with vapor). (See Fig. 1a for the positions of An, Mel/Geh, and Wo.)

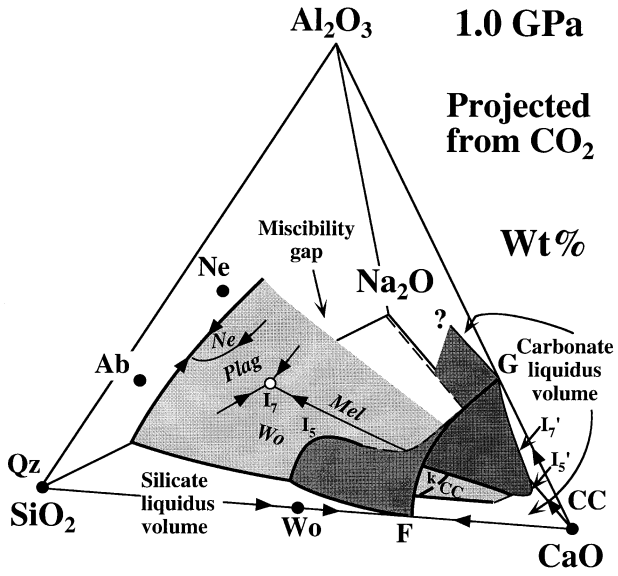

Fig. 11. Compositional tetrahedron showing the three major liquidus features, the miscibility gap (in Fig. 10b), silicate liquidus volume, and carbonate liquidus volumes. Possible cooling directions for some field boundaries are indicated by arrows. F is the eutectic e for the join Wo–CC in Fig. 2, and G is a hypothetical eutectic between Al_2O_3 and $CaCO_3$, located at ~30 wt % CaO. The carbonate liquidus volume near the CaO corner is for calcite, and its range becomes more limited at higher alkali contents, involving sodic carbonate minerals (e.g. nyerereite, Na_2CO_3).

CRYSTALLIZATION PATHS OF CARBONATED SILICATE LIQUIDS IN MODEL SYSTEM

Lee & Wyllie (1996) reviewed possible crystallization paths of carbonated silicate liquids using the phase relationships intersected by Ab–CC at 2·5 and 1·0 GPa emphasizing the variations with composition (nepheline- or quartz-normative, Ca/Na) and pressure. The evolution of carbonated silicate liquids towards carbonatitic residua is constrained not only by the liquid miscibility gap, but also by the silicate–carbonate liquidus field boundary. Lee & Wyllie (1996) considered these limits for the pseudoternary system in Fig. 2, and in Fig. 9b we extend the Ab–Wo liquidus field boundary to eutectic I_6. Here we compare the 1·0 GPa conclusions (from Figs 2 and 9b) with the corresponding pseudoternary paths for the new results from the $Ne_{90}Ab_{10}$–CC join (Figs 8 and 9a), and then illustrate more clearly the effect of composition by combining the results in the pseudoquarternary system (Fig. 11).

The pseudoternary system through Ab–$CaCO_3$–Na_2CO_3

Original silicate–CO_2 liquids in Fig. 9b precipitating silicate minerals Ab or Wo may:

(1) reach the field boundary m–I_5 and exsolve immiscible carbonate-rich liquid Lc (n–I_5'), then cool with composition changing toward eutectic I_6 while the carbonate-rich immiscible liquid similarly changes toward I_6';

(2) reach the silicate–carbonate field boundary Wo–CC and coprecipitate wollastonite and calcite until the liquid reaches I_5, where carbonate-rich liquid I_5' is exsolved; liquid I_5 will then change composition to the eutectic at I_6, exsolving Lc changing from I_5' to I_6';

(3) terminate at eutectics on the silicate–CO_2 liquidus with precipitation of silicate minerals and evolution of

CO_2. There are insufficient experimental data to evaluate this possibility.

The most calcic carbonate-rich liquid that could be produced is I_5' (70 wt % CaO in Fig. 2; maximum 73 wt % $CaCO_3$), but the silicate liquids trend towards I_6, which produces a much more sodic carbonate liquid I_6'. There are no crystallization paths for silicate–CO_2 liquids to produce carbonate-rich liquids between I_5 and I_5'.

The exsolved carbonate-rich liquids Lc along I_5'–I_6'–n precipitate only silicates (Wo and Ab) as long as they remain in equilibrium with the silicate liquids (except at I_5', where wollastonite is joined by calcite). If Lc is removed from the coexisting Ls, then the liquid can cool down the narrow, steep silicate liquidus surface I_5'–n–o until it reaches the silicate–carbonate field boundary I_5'–o, where a carbonate mineral is coprecipitated. These liquids will follow paths probably close to those determined in the carbonate system by Cooper *et al.* (1975) at lower pressures, with final liquids containing approximately equal proportions of $CaCO_3$ and Na_2CO_3.

The pseudoternary system through $Ne_{90}Ab_{10}$–$CaCO_3$–Na_2CO_3

The major difference between the pseudoternary systems based on Ab (Figs 2 and 9b) and Ne (Figs 8 and 9a) is that the silicate–carbonate field boundary in the latter system does not intersect the miscibility gap field boundary, with the consequence that the silicate liquidus surface completely surrounds the miscibility gap, and all immiscible consolute liquids, Ls and Lc, precipitate only silicate minerals. A second difference is that in the Ne-based system the silicate–carbonate field boundary passes much closer to the CaO corner than in the Ab system, causing expansion of the silicate liquidus fields (melilite), and contraction of the calcite liquidus field (Fig. 9).

Let us consider the crystallization paths for silicate–CO_2 liquids with primary minerals Ne, An, or Mel. Liquid paths may:

(1) reach the field boundary K–I_2–I_1–M, and exsolve immiscible carbonate-rich liquid Lc (K–I_2'–I_1'–N); the immiscible carbonate-rich liquids tend to be concentrated into the region of I_1' (76 wt % CaO; maximum 77 wt % $CaCO_3$);

(2) reach the field boundary for anorthite–melilite *en route* to the miscibility gap at I_2, after which they may continue to I_1, as in path (1) above; there is probably a thermal maximum across the melilite liquidus field from K to Mel, preventing the silicate-rich liquids from reaching the silicate–carbonate field boundary for melilite–calcite;

(3) terminate at undetermined eutectics on the silicate–CO_2 liquidus with precipitation of silicate minerals and evolution of CO_2.

Exsolved carbonate-rich liquids with compositions between N and K would not precipitate carbonates as long as they remained in equilibrium with the silicate-rich liquids. Crystallization paths of the liquids Lc when removed from the silicate liquids would pass down the steep liquidus surface with precipitation of combinations of nepheline, anorthite and melilite until they reached the silicate–carbonate liquidus field boundary, I_4–I_3–O in Figs 8 and 9a, where the silicate minerals would be joined by calcite. The liquid I_4 on the silicate–carbonate field boundary is richer in $CaCO_3$ than the immiscible liquids, containing ~85 wt % $CaCO_3$. The crystallization path would then continue along I_3–O toward residual liquids precipitating alkali carbonates such as nyerereite (Cooper *et al.*, 1975).

The pseudoquaternary system Na_2O–CaO–Al_2O_3–SiO_2 with excess CO_2

The paths of silicate–CO_2 liquids in Fig. 9a and b discussed above assume ternary phase relationships. In fact, although the liquidus relationships are close to ternary, liquid paths diverge from the triangular planes when silicate minerals are precipitated. Therefore, crystallization paths are better described in the CO_2-saturated, pseudoquaternary system Na_2O–CaO–Al_2O_3–SiO_2, as in Figs 10b and 11. Possible field boundaries for immiscible liquids on the shaded surface show the transition between the conditions described above for the two pseudoternary systems (Fig. 10b). Volumes, surfaces and lines extend into the tetrahedron from the areas, lines and points on the miscibility gap surface (Fig. 11). These phase relationships are needed (but unknown) in order to trace in detail the paths of crystallization from original silicate–CO_2 melts.

Original liquids in the silicate–CO_2 liquidus volume of Fig. 11 follow paths leading to similar residual products to those outlined above for the pseudoternary systems, with additional variations now apparent. Let us consider silicate liquids with primary nepheline, plagioclase, wollastonite or melilite.

(1) These liquids may follow paths to the miscibility gap surface where carbonate-rich liquid is exsolved, and they may migrate to the invariant point I_7 where the coexisting liquid Lc has composition I_7', between I_2' and I_6' in Figs 2, 8, and 9.

(2) There is no obvious path to the silicate–carbonate liquidus surface visible in Fig. 11. The path which appeared possible across the wollastonite liquidus in Figs 2 and 9b appears to be precluded by the rising liquidus temperature from I_7 along the field boundary between melilite and wollastonite. However, the possibility is real, as confirmed by the liquidus along the edge quartz–calcite (Fig. 11; Lee *et al.*, 1994).

(3) The phase relationships associated with the field boundary extending from I_7 into the silicate liquidus volume provide conditions for liquids which solidify to yield silicate minerals and CO_2 without immiscible liquids or coprecipitation of calcite.

The formation of immiscible liquids Lc (except those on the field boundary between Wo and CC, Fig. 10b), if they are separated from the host silicate liquid Ls, is followed by the precipitation of silicates only. The sequence of crystallization is controlled by the arrangement of field boundaries associated with I_1', I_2', I_5', I_6' and I_7' on the Lc surface, until the liquids reach the silicate–carbonate liquidus surface to the right and rear of Fig. 11. There, most of the liquids will coprecipitate calcite, but some original silicate liquids could yield immiscible sodic liquids (e.g. I_6') and coprecipitate nyerereite or gregoryite before calcite.

Of particular significance for the origin of carbonatite magmas are the surfaces enclosing the liquidus volume for the primary crystallization of calcite (and other carbonates). This volume is enclosed in Fig. 11 by the sides of the tetrahedron extending from CaO, by the silicate–carbonate liquidus surface, and by the lower portion of the miscibility gap surface with primary calcite (compare Fig. 10b). Silicate–CO_2 liquids may follow paths to this surface by two routes: (1) precipitation of silicates, liquid immiscibility, continued precipitation of silicates, and finally coprecipitation of calcite and alkali carbonates with silicates; or (2) precipitation of silicates, and then coprecipitation of calcite, which may be followed by liquid immiscibility and paths corresponding to those in (1).

Original silicate–CO_2 liquids can generate carbonate-rich liquids with compositions on the surface of the shaded carbonate volume, but it is impossible for liquids to follow paths inside this volume. Therefore, this is a forbidden volume for carbonatite magmas in this model system at 1·0 GPa.

Crystallization paths and haplocarbonatite magmas

The different kinds of paths of crystallization likely to be experienced by silicate–CO_2 liquids of various compositions have been identified from the phase diagrams in Figs 2, 8 and 11. Figure 11 provides a topological framework for tracing paths of crystallization leading to haplocarbonatite magmas. This overall view of the phase relationships facilitates the interpretations of results from individual rock studies, which sample only a small fraction of the phase fields. The phase diagrams also permit tests of the feasibility of hypotheses published during the debates of the 1980s, which tended to be based on petrography rather than phase diagrams, and on petrological imaginations as admirably fertile as some mantle samples. We emphasize that although our model system compositions differ from those of natural rocks, the topology of the main phase elements illustrates particular processes and insights about their controls. The phase geometry and minerals vary as a function of pressure and composition (especially Mg/Ca).

We now consider the generation of haplocarbonatite magmas in the model system, selecting only the starting compositions corresponding to carbonated silicate magmas (at temperatures on the liquidus, not above it) which follow differentiation paths that intersect the miscibility gap before they reach the silicate–carbonate liquidus boundary. They may follow two different types of sequences of crystallization, outlined below in stages. Each stage involves a temperature interval:

Stage 1: Ls + silicates. Ls is within the silicate liquidus volume (Fig. 11), represented in part by the silicate liquidus surfaces of Figs 2, 8 and 9. When Ls reaches the miscibility gap, the assemblage is joined by Lc.

Stage 2: Ls + Lc + silicates. Ls and Lc change compositions across the miscibility gap surface in Fig. 11, visualized in part by the intersections of Ls in boundaries m–I_5 and M–K, and of Lc in boundaries n–I_5' and N–K (Figs 2, 8 and 9). Crystallization of silicates and the exsolution of Lc can be followed by either (a) the exhaustion of Ls (or the fractional separation of Lc before Ls is used up), or (b) the precipitation of calcite, leading to Stage 3a or 3b.

Stage 3a: Lc + silicates. Liquid Lc will cool across the silicate liquidus surface represented by the areas I_5'–n–o and K–I_2'–I_1'–N–O–I_3–I_4–E (Figs 2 and 8; not clearly displayed in Fig. 11). The surfaces are steep, and the amount of precipitation is small. Although Lc is carbonate rich, it cannot precipitate carbonate minerals until it reaches the silicate–calcite field boundary, and Stage 4.

Stage 3b: Ls + Lc + silicates + calcite. This stage corresponds to Ls reaching the limiting silicate–calcite field boundary on the miscibility gap surface between Wo and CC in Figs 10b and 11, the locus of points corresponding to I_5 and I_5' in Figs 2 and 9b; this is the curve of intersection of the miscibility gap and the silicate–carbonate liquidus boundary surface. As in Stage 2, Ls will become used up, or exsolved Lc may be physically separated from Ls, and the remaining assemblage is then represented by the silicate–calcite field boundary in Stage 4.

Stage 4: Lc + silicates + carbonates. Liquid Lc, now corresponding to a haplocarbonatite magma, changes composition along the silicate–carbonate field boundary surface, visualized in part by surface intersections shown by the field boundaries I_5'–o and E–I_4–I_3–O (Figs 2 and 8; not clearly displayed in Fig. 11). This surface is physically separated from the miscibility gap surface except along the line of intersection of the two surfaces (between Wo and CC in Figs 10b and 11) corresponding to Stage 3b. Crystallization is dominated by calcite,

except for original liquids with very high peralkalinity (Kjarsgaard *et al.*, 1995). In a natural system calcite would form cumulates (it sinks even in experimental capsules, Fig. 4d; Wyllie & Tuttle, 1960). The residual liquid must be driven toward alkali carbonates (Cooper *et al.*, 1975), but Kjarsgaard *et al.* (1995) pointed out that the liquids so derived do not match some definitive characteristics of natural natrocarbonatites. There would be ample opportunity for the residual low-viscosity alkalic carbonatite magma to escape as a fenitizing fluid.

Three of the issues debated in the 1980s were: (1) Are silicate- and carbonate-rich liquids which do not mix at temperatures above their liquidi really conjugate liquids? (2) Are immiscible carbonate-rich liquids in experimental studies 'superheated' compared with natural carbonatite magmas? (3) Are natrocarbonatite magmas derived from parental Ca- and Mg-carbonate magmas, or vice versa? Some aspects of the debates are clarified and resolved unambiguously by the phase diagrams. The positions of those engaged in these debates have shifted through time, and the following quotations from recent papers will suffice as reviews. Barker (1996*a*) referred to 'The carefully reasoned debate between M. J. Le Bas (1987, 1989) and J. Gittins (1989; Twyman & Gittins, 1987)' as 'recommended reading', illustrating the complex problems in carbonatite petrogenesis. He cited recent petrographic observations favoring liquid immiscibility in lavas (Dawson *et al.*, 1992; Macdonald *et al.*, 1993; Church & Jones, 1995), and recalled the arguments that these may not be 'true immiscibility', but a reluctance of two liquids at different temperatures to mix.

The immiscibility issue, (1), and the 'superheat' issue, (2), were dealt with by Kjarsgaard *et al.* (1995, pp. 178–179), and they correctly concluded that this is not a problem at all. Twyman & Gittins (1987) had suggested that the occurrence of immiscibility in the Freestone & Hamilton (1980) experiments proved nothing and was an artifact of melting rocks with sharply divergent liquidi (natrocarbonatite ~500°C; silicate ~1000°C), i.e. the liquids are immiscible but do not represent a conjugate pair because they did not exist as a homogeneous, high-temperature liquid. Both Le Bas (1981, 1987, 1989) and Twyman & Gittins (1987) noted that 'the carbonate liquids ... were exsolved at temperatures 350–550°C hotter ('superheated') than the liquidus temperature of natrocarbonatite'. Kjarsgaard *et al.* (1995) reported experiments using a natural wollastonite nephelinite lava and synthetic natrocarbonatite. They used a pseudobinary system to illustrate the sequence of phase assemblages produced experimentally, and demonstrated the coexistence of silicate and alkalic carbonate liquids as conjugate pairs at 750°C and 700°C with melanite garnet, clinopyroxene and other silicate and oxide minerals, which confirmed that the carbonate liquid was not 'superheated'. The carbonate liquid compositions contained low but appreciable concentrations of Si, Ti, Al, Fe and Mg. No carbonate minerals were produced.

The experimental results on mixtures of natural rocks with carbonates presented by Kjarsgaard & Peterson (1991), Hamilton & Kjarsgaard (1993), and Kjarsgaard *et al.* (1995) can be more fully illustrated in terms of paths of crystallization in the framework of the comprehensive phase diagrams of Figs 2, 8 and 11, although the liquid compositions and minerals differ in detail, and the pressures are different. The product of Kjarsgaard *et al.* (1995) at the lowest temperature (700°C) corresponds to a liquid Lc on the surface passing through field boundaries I_5'–n and K–N (Figs 2, 8 and 9), about midway between CaO and Na_2O, and still in equilibrium with the silicate liquid, Ls, and silicate minerals. They recognized that the immiscible haplonatrocarbonatite magma would not precipitate carbonates without further fractionation of silicates, concluding (p. 184): 'One can envisage efficient fractionation of these ferromagnesian solids concurrent with the separation of exsolved carbonate liquids from their silicate liquid host.' According to the phase diagrams (Figs 2 and 8), these two processes are not concurrent—the exsolved carbonate liquids Lc must first be physically separated from the silicate host magma Ls before they become capable of fractionating down the silicate liquidus to reach the silicate–carbonate liquidus surface (passing through I_5'–o and I_3–O, Figs 2, 8, and 9).

Kjarsgaard & Peterson (1991; using a pseudobinary diagram) and Hamilton & Kjarsgaard (1993; using a Hamilton projection) reported a sequence of phase assemblages (neglecting oxides) obtained from two sets of experiments using Shombole lavas $\pm$ added $CaCO_3$, which correspond as follows to the stages outlined above: Ls; Stage 2, Ls + Lc + silicates; and Stage 3b, Ls + Lc + silicates + calcite. The liquid composition paths plotted by Hamilton & Kjarsgaard (1993) are reasonably consistent with the miscibility gap field boundaries in Figs 2 and 8 (considering the differences in bulk composition and pressure), diverging from K with decreasing temperature from 1025°C to 900°C. The 900°C silicate liquid is greatly enriched in $(Na_2O + SiO_2)/CaO$. This liquid composition is constrained by the phase assemblage (Stage 3b) to lie on the curve of intersection of the miscibility gap surface and the silicate–carbonate liquidus (Figs 10b and 11). This indicates that for the natural rock compositions used in the experiments, the primary calcite field on the miscibility gap surface extends very close to the side (SiO_2–Na_2O–Al_2O_3) of the pseudoquaternary system in Fig. 11; the calcite liquidus volume is similarly greatly expanded to low CaO contents compared with that depicted in Fig. 11.

With respect to the third issue, according to Barker (1996*a*), 'Le Bas (1987, 1989) championed natrocarbonatite liquid as parent to the more Ca- and Mg-rich carbonate liquids, whereas Gittins (1989; Twyman

& Gittins, 1987) concluded that natrocarbonatite liquid is a product of extreme fractionation of Ca- and Mg-rich parental liquid.' Le Bas (1981, 1987) appealed to a superheated immiscible alkalic carbonatite magma which lost alkalis, becoming a calcite–dolomite liquid as it cooled through ~500°C, followed by crystallization of calcitic and dolomitic carbonatites. As discussed above, the phase diagrams show that an immiscible liquid would not be superheated, but it would be in equilibrium with primary silicate minerals. If this liquid cooled through 500°C or so as Le Bas proposed, it would precipitate a small amount of silicate minerals and reach the silicate–carbonate liquidus boundary; this is unlikely to be associated with much change of Ca/Na in the liquid. The silicate–carbonate liquidus boundary in Fig. 11 (shaded surface near CaO–Na_2O) is so close to the carbonate join ($CaCO_3$–Na_2CO_3) that its temperature profile must be very similar to that in the carbonate system. The liquidus temperature drops continuously and steeply from $CaCO_3$ toward natrocarbonatite compositions. We cannot construct reasonable paths of crystallization which would generate residual calciocarbonatite magmas from a high-temperature immiscible natrocarbonatite magma.

Both Le Bas (1981, 1987) and Gittins (1989) have proposed that an alkalic carbonatite magma derived either by immiscibility from nephelinite magma (Le Bas, 1981) or by fractional crystallization of calciocarbonatite (Gittins, 1989) could lose alkalis through the formation and removal of a fluid phase (causing fenitization), and thus become enriched in Ca/Na, differentiating toward a calciocarbonatite magma. It can be shown with model phase diagrams that the crystallizing liquid would not be turned significantly in the direction of increasing Ca/Na content if it evolved an alkali-rich vapor phase. The system would simply retain the appropriate Ca/Na distribution between solid, liquid and vapor by precipitating more minerals. As the alkalic carbonatite magma evolves the fenitizing fluids, the liquid crystallizes with little change in composition, producing solid sövite. There is agreement that fenitization involves the extraction of alkalis from a carbonatite magma, but this does not require that the magma changes composition toward calciocarbonatite.

PETROLOGICAL APPLICATIONS AND CONCLUSIONS

The following applications are presented with the caution associated with the application of results from a simple model system to magmatic systems (Lee & Wyllie, 1996). The results from model systems provide information on the kinds of processes which are possible, and those which are impossible. The existence of a possible process is no guarantee that it will actually occur in a magmatic system. The constraints from phase equilibria complement those provided by field petrology and geochemistry. Detailed reviews of the three approaches are contained in recent books (Bell, 1989; Bell & Keller, 1995).

Barker (1996*a*, *b*) recently reviewed carbonatite volcanism, and the effects of carbonatite magmas within the upper mantle. He found support for the hypothesis that many carbonatites were primary magmas from the mantle, rather than derivative from silicate magmas within the crust, the process which he previously preferred on the basis of field relationships in alkaline complexes (Barker, 1989). Bailey (1993) reached similar conclusions, favoring primary calciocarbonatite magmas from the mantle. Bell & Blenkinsop (1989) and Bell & Dawson (1995) concluded from neodymium and strontium isotopic studies that parental magmas of carbonatites were produced from commonly ancient depleted mantle. In several occurrences the rocks could not have been derived from a single isotopically homogeneous source, as at least two sources were required. Although Lee & Wyllie (1997) concluded that primary magmas from the mantle were possible, their conclusions from phase relationships were inconsistent with a primary melt being calciocarbonatitic in composition, and primary natrocarbonatites were unlikely to occur. Primary magmas should be dominated by calcic dolomite. Lee & Wyllie suggested that carbonatitic magmas from the mantle should exhibit intrusive and eruptive styles similar to those of kimberlites, because of their probable small volume, their fluidity, and gas evolution during uprise [following Wyllie & Huang (1976) and Wyllie (1989), and consistent with Eggler (1989)].

There is field and petrographic evidence for the formation of immiscible carbonatite liquids (e.g. Kjarsgaard & Peterson, 1991; Dawson *et al.*, 1994, 1996; Church & Jones, 1995), and the intervention of liquid immiscibility in the formation of carbonatite magmas is strongly favored by many (see Bell, 1989; Bell & Keller, 1995). Many alkali rocks (e.g. nephelinites, phonolites, and ijolites) from carbonatite complexes do project near the silicate-rich limb of a miscibility gap in a Hamilton projection (Le Bas, 1987; Kjarsgaard & Hamilton, 1989). There are also natural examples confirming crystallization paths that led from silicate liquidus to silicate–calcite field boundaries (e.g. Watson, 1967). Donaldson & Reid (1982) presented a detailed petrographic account of a narrow, banded kimberlite dyke associated with the de Beers mine kimberlite pipe. This dyke contained groundmass calcite and calcite in elongate amygdales aligned at right angles to the dyke walls. The vesicle filling was attributed to a residual fluid of carbonatite composition derived from progressive crystallization of the kimberlite melt. Exley & Jones (1983) found with

trace elements and Sr isotope ratios that some of the calcite in the dyke (both in the groundmass and in certain amygdales) had precipitated from residual kimberlite liquid, whereas that in other amygdales was of secondary origin. They also showed that the primary calcites had high Sr and Ba and low $^{87}Sr/^{86}Sr$ ratios, indicating that these shared chemical characteristics with carbonate in carbonatites.

The system Na_2O–CaO–Al_2O_3–SiO_2–CO_2 is not relevant for most mantle processes and products, but it includes compositions representing some evolved nephelinites and phonolites, calciocarbonatites, and natrocarbonatites. The different types of differentiation paths of carbonated alkalic silicate magmas depend on the original liquid composition, the distribution of liquidus field boundaries, and the distribution of thermal maxima on the liquidus. The petrological problems which can be addressed are presented as a series of questions, some of which were considered by Lee & Wyllie (1996) using Figs 2 and 9b as guides. We can now evaluate them with another dimension, using Figs 9, 10 and 11.

Can calcite spherules or ocelli in mantle xenoliths represent magma compositions? Calcite spherules in mantle xenoliths have been interpreted as representing immiscible carbonate liquids (e.g. Pyle & Haggerty, 1994; Seifert & Thomas, 1995; Kogarko *et al.*, 1995*a*). The size of the calcite liquidus volume illustrated in Figs 9, 10 and 11 shows that no silicate-derived carbonatitic magma can have composition with >85 wt % $CaCO_3$, and such a liquid cannot solidify completely to a 99 wt % calcite spherule. Lee *et al.* (1994) and Lee & Wyllie (1996, 1997) maintained that the reported calcite spherules probably represented rounded crystalline calcite grown from a silicate–carbonate magma. This conclusion was supported with phase diagrams, and with previous descriptions of rounded calcite crystals grown experimentally in melts of varied composition. Rounded carbonate crystals are also known in lavas, e.g. gregoryite (with oscillatory zoning) in natrocarbonatite flows at Oldoinyo Lengai (Cooper *et al.*, 1975; Church & Jones, 1995).

What is the maximum percentage of $CaCO_3$ in immiscible carbonatite magmas? We see no evidence for >80 wt % $CaCO_3$ in Hamilton projections of experimental results (Figs 2 and 8; Hamilton & Kjarsgaard, 1993; Macdonald *et al.*, 1993; Lee & Wyllie, 1997, with MgO added). Hamilton & Kjarsgaard (1993) reported immiscible liquids reaching 90 wt % $CaCO_3$ when plotted in terms of carbonate components only, but when the presence of silicate components is taken into account, they plot the same point in a Hamilton projection which corresponds to a composition with no more than 75 wt % $CaCO_3$, consistent with the other published miscibility gaps.

What conditions and processes can lead to the formation of carbonatite magmas from alkalic parent magmas? As shown above, carbonatite magmas are formed when (1) the silicate magma reaches the miscibility gap, or (2) the silicate magma differentiation path bypasses thermal maxima and reaches the silicate–calcite liquidus boundary under conditions where this boundary does not intersect the miscibility gap; this permits the liquid to continue differentiating toward $CaCO_3$ (as in Figs 8 and 11; contrast Fig. 2).

What carbonatite magma compositions can be derived from alkalic parent magmas? In general, the higher the Na/Ca in the silicate magma, the more sodic the immiscible carbonate-rich magma (Fig. 9), but the Al/Si ratio is also influential (compare tie-lines I_6–I_6' and I_1–I_1' in Fig. 9). Kjarsgaard & Peterson (1991) emphasized the importance of peralkalinity on the compositions of immiscible carbonate-rich liquids. The immiscible carbonate-rich liquids separated from many starting silicate compositions tend to be concentrated in the region I_1', I_2', I_5', and I_7' (Figs 8, 9, 10 and 11). These are calciocarbonatite magmas, with somewhat less than 80 wt % $CaCO_3$ but with significant contents of alkalis (up to 20 wt % or more Na_2CO_3). For some high-alkali evolved (low-MgO) silicate magmas, there is a prospect of generating more sodic immiscible carbonatite magmas (I_6–I_6' in Fig. 9b), which could produce natrocarbonatites with compositions considerably richer in Na_2O than nyerereite (Nye, Fig. 1). Kjarsgaard *et al.* (1995) demonstrated that immiscible natrocarbonatite liquids could be produced on both sides of the nyerereite–fairchildite thermal divide. Therefore, natrocarbonatites corresponding to those at Oldoinyo Lengai which precipitate gregoryite can be produced by liquid immiscibility from an alkali silicate parent.

What crystallization paths are followed by derivative carbonatite magmas? Some interesting questions about fractionation of carbonatite magmas cannot be evaluated here, because our system contains neither Mg nor Fe; we are concerned with variations in amount of carbonates, Ca/Na, and Al/Si. Carbonatite magmas precipitate calcite only when they reach the silicate–calcite liquidus boundary, either by direct crystallization without immiscibility, or via the miscibility gap. Some liquids cool down the steep silicate liquidus (connecting the area between K–I_2'–I_1'–N and I_4–I_3–O in Fig. 8 with I_5'–n–o in Fig. 2) until they reach the boundary represented by the shaded surface behind the sharp bend below G in Fig. 11. The carbonatite magma compositions are concentrated in the range I_4, I_3 to I_5' (Figs 2, 8, and 9), but for peralkaline compositions they may extend to significantly more sodic compositions near I_6' (Figs 2, 9, and 10). Differentiation along the silicate–carbonate liquidus boundary (under conditions where it does not intersect the miscibility gap, Figs 8 and 9a) can yield melts corresponding to calciocarbonatites (e.g. near I_4, I_3 in Figs 8 and 9a). The results of Cooper *et al.* (1975) in the model system $CaCO_3$–Na_2CO_3–K_2CO_3

demonstrate that fractional crystallization of alkali-bearing calciocarbonatite magmas must follow paths along the shaded surface between CaO and Na_2O in Fig. 11 (I_4–I_3–O and I_5'–o in Fig. 9) toward natrocarbonatite compositions, but fractionating calciocarbonatite liquids are prevented by a thermal barrier from reaching compositions which precipitate gregoryite. Either this barrier is bypassed in a more complex system, or Oldoinyo Lengai lavas are not produced by fractional crystallization of calciocarbonatite magma. Alkali carbonate immiscible liquid from peralkaline magma may fractionate to either side of the thermal barrier (Kjarsgaard *et al.*, 1995).

Can primary natrocarbonatite magmas differentiate to calciocarbonatites by fractional crystallization? We could find no reasonable paths of crystallization which would pass from high-temperature natrocarbonatite magmas to calciocarbonatite magmas. We conclude that calciocarbonatite magmas must generate residual alkali-rich carbonatite magmas (which precipitate calcite and a trace of silicate minerals, i.e. sövite).

Can primary natrocarbonatite magmas differentiate to calciocarbonatites by evolution of vapor? The proposal of Gittins (1989) and others that extraction of alkali-rich vapor or fluid (involving H_2O or halides or both) would lead to reversals of the magma's crystallization trend back toward enrichment in $CaCO_3$ is inconsistent with phase relationships in model systems. The effect would be to cause precipitation of calcite (sövite), with little change in liquid composition.

What is the effect of a modest amount of water or halogens on the phase relations in the model systems? Liquidus temperatures would be slightly lowered, and solidus temperatures could be significantly lowered, with the amount of liquid present at the lowest temperatures being more or less a function of the amount of the additional components. Minerals containing these components would precipitate at lower temperatures. The relative compositions of the volumes, surfaces and lines depicted in Fig. 11 would change, but we do not believe that the topology would change significantly. Baker & Wyllie (1990) found that 4·5 wt % H_2O added to their nephelinite–carbonate mixtures at 2·5 GPa reduced the liquidus temperature and the size of the silicate–carbonate miscibility gap. Lee & Wyllie (1994) found that with excess H_2O on the join $Ne_{90}Ab_{10}$–CC at 0·1 GPa, the liquidus temperature was lowered sufficiently for residual liquid paths to pass, in effect, below the high-temperature miscibility gap, along the silicate–carbonate–vapor liquidus field boundary. Jago & Gittins (1991) assigned a major role to fluorine in carbonatite genesis. The phase relationships in more complex systems including modest amounts of H_2O and F would reveal modified paths of crystallization, but we do not believe they would invalidate any of those revealed in Figs 2, 8 and 11.

ACKNOWLEDGEMENTS

We thank K. Bell and C. H. Donaldson for helpful comments. The manuscript has also benefited from constructive reviews by A. P. Jones, B. A. Kjarsgaard, and an anonymous reviewer. This research was supported by the Earth Science section of the US National Science Foundation Grant EAR-921886. This is Contribution 5916 of the Division of Geological and Planetary Sciences, California Institute of Technology.

REFERENCES

Bailey, D. K., 1993. Carbonate magmas. *Journal of the Geological Society, London* **150,** 637–651.

Baker, M. B. & Wyllie, P. J., 1990. Liquid immiscibility in a nephelinite–carbonate system at 25 kbars and implications for carbonatite origin. *Nature* **346,** 168–170.

Barker, D. S., 1989. Field relations of carbonatites. In: Bell, K. (ed.) *Carbonatites: Genesis and Evolution*. London: Unwin Hyman, pp. 38–69.

Barker, D. S., 1996*a*. Carbonatite volcanism. In: Mitchell, R. H. (ed.) *Undersaturated Alkaline Rocks: Mineralogy, Petrogenesis, and Economic Potential. Mineralogical Association of Canada, Short Course* **24,** 45–61.

Barker, D. S., 1996*b*. Consequences of recycled carbon in carbonatites. *Canadian Mineralogist* **34,** 373–387.

Bell, K. (ed.), 1989. *Carbonatites: Genesis and Evolution*. London: Unwin Hyman.

Bell, K. & Blenkinsop, J., 1989. Neodymium and strontium isotope geochemistry of carbonatites. In: Bell, K. (ed.) *Carbonatites: Genesis and Evolution*. London: Unwin Hyman, pp. 278–300.

Bell, K. & Dawson, J. B., 1995. Nd and Sr isotope systematics of the active carbonatite volcano, Oldoinyo Lengai. In: Bell, K. & Keller, J. (eds) *Carbonatite Volcanism: Oldoinyo Lengai and the Petrogenesis of Natrocarbonatites. IAVCEI Proceedings in Volcanology 4*. Berlin: Springer-Verlag, pp. 100–112.

Bell, K. & Keller, J. (eds), 1995. *Carbonatite Volcanism: Oldoinyo Lengai and the Petrogenesis of Natrocarbonatites. IAVCEI Proceedings in Volcanology 4*. Berlin: Springer-Verlag.

Bell, P. M. & Roseboom, E. H., 1969. Melting relationships of jadeite and albite to 45 kilobars with comments on the melting behavior of binary systems at high pressures. In: Papike, J. J. (ed.) *Pyroxenes and Amphiboles: Crystal Chemistry and Phase Petrology. Mineralogical Society of America Special Paper* **2,** 151–161.

Boettcher, A. L. & Wyllie, P. J., 1969. The system CaO–SiO_2–CO_2–H_2O: III. Second critical end-point on the melting curve. *Geochimica et Cosmochimica Acta* **33,** 611–632.

Bowen, N. L., 1912. The binary system: $Na_2Al_2Si_3O_8$ (nephelite, carnegieite)–$CaAl_2Si_2O_8$ (anorthite). *American Journal of Science* **33,** 551–573.

Boyd, F. R. & England, J. L., 1963. Effect of pressure on the melting of diopside, $CaMgSi_2O_6$, and albite, $NaAlSi_3O_8$, in the range up to 50 kilobars. *Journal of Geophysical Research* **68,** 311–323.

Brooker, R. A. & Hamilton, D. L., 1990. Three-liquid immiscibility and the origin of carbonatites. *Nature* **346,** 459–462.

Church, A. A. & Jones, A. P., 1995. Silicate–carbonate immiscibility at Oldoinyo Lengai. *Journal of Petrology* **36,** 869–889.

Cooper, A. F., Gittins, J. & Tuttle, O. F., 1975. The system Na_2CO_3–K_2CO_3–$CaCO_3$ at 1 kilobar and its significance in carbonatite petrogenesis. *American Journal of Science* **275,** 534–560.

Dalton, J. A. & Wood, B. J., 1993. The compositions of primary carbonate melts and their evolution through wallrock reaction in the mantle. *Earth and Planetary Science Letters* **119,** 511–525.

Dawson, J. B., Smith, J. V. & Steele, I. M., 1992. 1966 ash eruption of the carbonatite volcano Oldoinyo Lengai: mineralogy of lapilli and mixing of silicate and carbonate magmas. *Mineralogical Magazine* **56,** 1–16.

Dawson, J. B., Pinkerton, H., Pyle, D. M. & Nyamweru, C., 1994. June 1993 eruption of Oldoinyo Lengai, Tanzania: exceptionally viscous and large carbonatite lava flows and evidence for coexisting silicate and carbonate magmas. *Geology* **22,** 799–802.

Dawson, J. B., Pyle, D. M. & Pinkerton, H., 1996. Evolution of natrocarbonatite from a wollastonite nephelinite parent: evidence from the June, 1993 eruption of Oldoinyo Lengai, Tanzania. *Journal of Geology* **104,** 41–54.

Donaldson, C. H. & Reid, A. M., 1982. Multiple intrusion of a kimberlite dyke. *Transactions of Geological Society of South Africa* **85,** 1–12.

Eggler, D. H., 1974. Effect of CO_2 on the melting of peridotite. *Carnegie Institution of Washington, Yearbook* **73,** 215–224.

Eggler, D. H., 1976. Composition of the partial melt of carbonated peridotite in the system CaO–MgO–SiO_2–CO_2. *Carnegie Institution of Washington, Yearbook* **75,** 623–626.

Eggler, D. H., 1978. The effect of CO_2 upon partial melting of peridotite in the system Na_2O–CaO–Al_2O_3–MgO–SiO_2–CO_2 to 35 kb, with an analysis of melting in a peridotite–H_2O–CO_2 system. *American Journal of Science* **278,** 305–343.

Eggler, D. H., 1989. Carbonatites, primary melts, and mantle dynamics. In: Bell, K. (ed.) *Carbonatites: Genesis and Evolution*. London: Unwin Hyman, pp. 561–579.

Exley, R. A. & Jones, A. P., 1983. Sr^{87}/Sr^{86} in kimberlitic carbonates by ion microprobe—hydrothermal alteration, crustal contamination and relation to carbonatite. *Contributions to Mineralogy and Petrology* **83,** 288–292.

Franz, G. W. & Wyllie, P. J., 1967. Experimental studies in the system CaO–MgO–SiO_2–CO_2–H_2O. In: Wyllie, P. J. (ed.) *Ultramafic and Related Rocks*. New York: John Wiley, pp. 323–326.

Freestone, I. C. & Hamilton, D. L., 1980. The role of liquid immiscibility in the genesis of carbonatites—an experimental study. *Contributions to Mineralogy and Petrology* **73,** 105–117.

Gittins, J., 1989. The origin and evolution of carbonatite magmas. In: Bell, K. (ed.) *Carbonatites: Genesis and Evolution*. London: Unwin Hyman, pp. 580–600.

Goldsmith, J. R. & Newton, R. C., 1977. Scapolite–plagioclase stability relations at high pressures and temperatures in the system $NaAlSi_3O_8$–$CaAl_2Si_2O_8$–$CaCO_3$–$CaSO_4$. *American Mineralogist* **62,** 1063–1081.

Greig, J. W. & Barth, T. F. W., 1938. The system $Na_2O{\cdot}Al_2O_3{\cdot}2SiO_2$ (nepheline, carnegieite)–$Na_2O{\cdot}Al_2O_3{\cdot}6SiO_2$ (albite). *American Journal of Science* **35A,** 93–112.

Hamilton, D. L. & Kjarsgaard, B. A., 1993. The immiscibility of silicate and carbonate liquids. *South African Journal of Geology* **96,** 139–142.

Heinrich, E. W., 1966. *The Geology of Carbonatites*. Chicago, IL: Rand McNally.

Huang, W.-L. & Wyllie, P. J., 1974. Eutectic between wollastonite II and calcite contrasted with thermal barrier in MgO–SiO_2–CO_2 at 30 kilobars, with applications to kimberlite–carbonatite petrogenesis. *Earth and Planetary Science Letters* **24,** 305–310.

Huang, W.-L., Wyllie, P. J. & Nehru, C. E., 1980. Subsolidus and liquidus phase relationships in the system CaO–SiO_2–CO_2 to 30 Kbar with geological applications. *American Mineralogist* **65,** 285–301.

Irving, A. J. & Wyllie, P. J., 1975. Subsolidus and melting relationships for calcite, magnesite, and the join $CaCO_3$–$MgCO_3$ to 36 kilobars. *Geochimica et Cosmochimica Acta* **39,** 35–53.

Jago, B. C. & Gittins, J., 1991. The role of fluorine in carbonatite magma evolution. *Nature* **349,** 56–58.

Keller, J., 1981. Carbonatite volcanism in the Kaiserstuhl alkaline complex: evidence for highly fluid carbonatitic melts at the Earth's surface. *Journal of Volcanology and Geothermal Research* **9,** 423–431.

Keller, J., 1989. Extrusive carbonatites and their significance. In: Bell, K. (ed.) *Carbonatites: Genesis and Evolution*. London: Unwin Hyman, pp. 70–88.

Kjarsgaard, B. A. & Hamilton, D. L., 1988. Liquid immiscibility and the origin of alkali-poor carbonatites. *Mineralogical Magazine* **52,** 43–55.

Kjarsgaard, B. A. & Hamilton, D. L., 1989. The genesis of carbonatites by immiscibility. In: Bell, K. (ed.) *Carbonatites: Genesis and Evolution*. London: Unwin Hyman, pp. 388–404.

Kjarsgaard, B. & Peterson, T., 1991. Nephelinite–carbonatite liquid immiscibility at Shombole Volcano, East Africa: petrographic and experimental evidence. *Mineralogy and Petrology* **43,** 293–314.

Kjarsgaard, B. A., Hamilton, D. L. & Peterson, T. D., 1995. Peralkaline nephelinite/carbonatite liquid immiscibility: comparison of phase compositions in experiments and natural lavas from Oldoinyo Lengai. In: Bell, K. & Keller, J. (eds) *Carbonatite Volcanism: Oldoinyo Lengai and the Petrogenesis of Natrocarbonatites. IAVCEI Proceedings in Volcanology 4*. Berlin: Springer-Verlag, pp. 163–190.

Kogarko, L. N., Henderson, C. M. B. & Pacheco, H., 1995*a*. Primary Ca-rich carbonatite magma and carbonate–silicate–sulfide liquid immiscibility in the upper-mantle. *Contributions to Mineralogy and Petrology* **121,** 267–274.

Kogarko, L. N., Kononova, V. A., Orlova, M. P. & Woolley, A. R., 1995*b*. *Alkaline Rocks and Carbonatites of the World. Part 2: Former USSR*. London: Chapman & Hall.

Koster van Groos, A. F., 1975. The effect of high CO_2 pressures on alkalic rocks and its bearing on the formation of alkalic ultrabasic rocks and the associated carbonatites. *American Journal of Science* **275,** 163–185.

Koster van Groos, A. F. & Wyllie, P. J., 1966. Liquid immiscibility in the system Na_2O–Al_2O_3–SiO_2–CO_2 at pressures to 1 kilobar. *American Journal of Science* **264,** 234–255.

Koster van Groos, A. F. & Wyllie, P. J., 1968. Liquid immiscibility in the join $NaAlSi_3O_8$–Na_2CO_3–H_2O and its bearing on the genesis of carbonatites. *American Journal of Science* **266,** 932–967.

Koster van Groos, A. F. & Wyllie, P. J., 1973. Liquid immiscibility in the join $NaAlSi_3O_8$–$CaAl_2Si_2O_8$–Na_2CO_3–H_2O. *American Journal of Science* **273,** 465–487.

Le Bas, M. J., 1977. *Carbonatite–Nephelinite Volcanism*. London: John Wiley.

Le Bas, M. J., 1981. Carbonatite magmas. *Mineralogical Magazine* **44,** 133–140.

Le Bas, M. J., 1987. Nephelinites and carbonatites. In: Fitton, J. G. & Upton, B. G. J. (eds) *Alkaline Igneous Rocks. Geological Society Special Publication* **30,** 53–83.

Le Bas, M. J., 1989. Diversification of carbonatite. In: Bell, K. (ed.) *Carbonatites: Genesis and Evolution*. London: Unwin Hyman, pp. 428–447.

Lee, W.-J. & Wyllie, P. J., 1992*a*. New data on CO_2-rich immiscible liquids in Na_2O–CaO–Al_2O_3–SiO_2–CO_2 from 25 to 1 kb: carbonatite genesis. *EOS* **73,** 349–350.

Lee, W.-J. & Wyllie, P. J., 1992*b*. Liquid immiscibility between silicates and carbonates must intersect suitable liquidus field boundaries to have petrogenetic significance. *Abstracts. 29th International Geological Congress, Kyoto*, p. 571.

Lee, W.-J. & Wyllie, P. J. 1992*c*. Silicate–carbonate liquid miscibility gaps, and liquidus field boundaries: carbonatites by immiscibility or fractionation. *EOS* **73,** 606.

Lee, W.-J. & Wyllie, P. J., 1994. Experimental data bearing on liquid immiscibility, crystal fractionation, and the origin of calciocarbonatites and natrocarbonatites. *International Geology Review* **36,** 797–819.

Lee, W.-J. & Wyllie, P. J., 1996. Liquid immiscibility in the join $NaAlSi_3O_8$–$CaCO_3$ to 2·5 GPa and the origin of calciocarbonatite magmas. *Journal of Petrology* **37,** 1125–1152.

Lee, W.-J. & Wyllie, P. J., 1997. Liquid immiscibility between nephelinite and carbonatite from 2·5 to 1·0 GPa compared with mantle melt compositions. *Contributions to Mineralogy and Petrology* **127**, 1–16.

Lee, W.-J., Wyllie, P. J. & Rossman, G. R., 1994. CO_2-rich glass, round calcite crystals and no liquid immiscibility in the system CaO–SiO_2–CO_2 at 2·5 GPa. *American Mineralogist* **79,** 1135–1144.

Maaloe, S. & Wyllie, P. J., 1975. The join grossularite–calcite through the system CaO–Al_2O_3–SiO_2–CO_2 at 30 kilobars: crystallization range of silicates and carbonates on the liquidus. *Earth and Planetary Science Letters* **28,** 205–208.

Macdonald, R., Kjarsgaard, B. A., Skilling, I. P., Davies, G. R., Hamilton, D. L. & Black, S., 1993. Liquid immiscibility between trachyte and carbonate in ash flow tuffs from Kenya. *Contributions to Mineralogy and Petrology* **114,** 276–287.

Otto, J. W. & Wyllie, P. J., 1993. Relationships between silicate melts and carbonate-precipitating melts in CaO–MgO–SiO_2–CO_2–H_2O at 2 kbar. *Mineralogy and Petrology* **48,** 343–365.

Pyle, J. M. & Haggerty, S. E., 1994. Silicate–carbonate liquid immiscibility in upper-mantle eclogites: implications for natrosilicic and carbonatitic conjugate melts. *Geochimica et Cosmochimica Acta* **58,** 2997–3011.

Seifert, W. & Thomas, R., 1995. Silicate–carbonate immiscibility: a melt inclusion study of melilitite and wehrlite xenoliths in tephrite from the Elbe Zone, Germany. *Chemie der Erde* **55,** 263–279.

Stoppa, F. & Lavecchia, G., 1992. Late Pleistocene ultra-alkaline magmatic activity in the Umbria–Latium region (Italy)—an overview. *Journal of Volcanology and Geothermal Research* **52,** 277–293.

Sweeney, R. J., 1994. Carbonatite melt compositions in the Earth's mantle. *Earth and Planetary Science Letters* **128,** 259–270.

Thibault, Y., Edgar, A. D. & Lloyd, F. E., 1992. Experimental investigation of melts from a carbonated phlogopite lherzolite: implications for metasomatism in the continental lithospheric mantle. *American Mineralogist* **77,** 784–794.

Tuttle, O. F. & Gittins, J., 1966. *Carbonatites*. New York: Interscience.

Twyman, J. D. & Gittins, J., 1987. Alkalic carbonatite magmas: parental or derivative? In: Fitton, J. G. & Upton, B. G. J. (eds) *Alkaline Igneous Rocks. Geological Society, London, Special Publication* **30,** 85–94.

Verwoerd, W. J., 1978. Liquid immiscibility and the carbonatite–ijolite relationship: preliminary data on the join $NaFe^{3+}Si_2O_6$–$CaCO_3$ and related compositions. *Carnegie Institution of Washington, Yearbook* **77,** 767–774.

Wallace, M. E. & Green, D. H., 1988. An experimental determination of primary carbonatite magma composition. *Nature* **335,** 343–346.

Watkinson, D. H., 1970. Experimental studies bearing on the origin of the alkalic rock–carbonatite complex and niobium mineralization at Oka, Quebec. *Canadian Mineralogist* **10,** 350–361.

Watkinson, D. H. & Wyllie, P. J., 1969. Phase equilibrium studies bearing on the limestone-assimilation hypothesis. *Geological Society of America Bulletin* **80,** 1565–1576.

Watkinson, D. H. & Wyllie, P. J., 1971. Experimental study of the join $NaAlSiO_4$–$CaCO_3$–H_2O and the genesis of alkalic rock–carbonatite complexes. *Journal of Petrology* **12,** 357–378.

Watson, K. D., 1967. Kimberlite of Eastern North America. In: Wyllie, P. J. (ed.) *Ultramafic and Related Rocks*. New York: John Wiley, pp. 312–323.

Woolley, A. R., 1987. *Alkaline Rocks and Carbonatites of the World. Part 1: North and South America*. London: British Museum (Natural History).

Wyllie, P. J., 1978. Mantle fluid compositions buffered in peridotite–CO_2–H_2O by carbonates, amphibole, and phlogopite. *Journal of Geology* **86,** 687–713.

Wyllie, P. J., 1989. Origin of carbonatites: evidence from phase equilibrium studies. In: Bell, K. (ed.) *Carbonatites: Genesis and Evolution*. London: Unwin Hyman, pp. 500–545.

Wyllie, P. J. & Haas, J. L., 1965. The system CaO–SiO_2–CO_2–H_2O: I. Melting relationships with excess vapor at 1 kilobar pressure. *Geochimica et Cosmochimica Acta* **29,** 871–892.

Wyllie, P. J. & Huang, W.-L, 1975. Peridotite, kimberlite, and carbonatite explained in the system CaO–MgO–SiO_2–CO_2. *Geology* **3,** 621–624.

Wyllie, P. J. & Huang, W.-L., 1976. Carbonation and melting reactions in the system CaO–MgO–SiO_2–CO_2 at mantle pressures with geophysical and petrological applications. *Contributions to Mineralogy and Petrology* **54,** 79–107.

Wyllie, P. J. & Tuttle, O. F., 1960. The system CaO–CO_2–H_2O and the origin of carbonatites. *Journal of Petrology* **1,** 1–46.